

Image biomarker standardisation initiative
feature definitions
version 1.3

Alex Zwanenburg Stefan Leger Martin Vallières Steffen Löck
on behalf of the image biomarker standardisation initiative

The image biomarker standardisation initiative

The image biomarker standardisation initiative (IBSI) is an independent international collaboration which works towards standardisation of image biomarkers. Reproducibility and validation of studies in quantitative image analysis/ radiomics is a major challenge for the field (Gillies et al., 2015; Hatt et al., 2016; Yip and Aerts, 2016). Standardisation of image biomarker definitions and image processing steps, and provision of clear reporting guidelines can address part of the issue.

Copyright

This work is licensed under the Creative Commons Attribution 4.0 International License. To view a copy of this license, visit <http://creativecommons.org/licenses/by/4.0/> or send a letter to Creative Commons, PO Box 1866, Mountain View, CA 94042, USA.

Contact

Dr. Alex Zwanenburg
alexander.zwanenburg@nct-dresden.de

IBSI collaborators

Mahmoud A. Abdalah	Department of cancer imaging and metabolism, Moffitt Cancer Center, Tampa (FL), USA
Hugo Aerts	Computational Imaging and Bioinformatics Laboratory, Dana-Farber Cancer Institute and Harvard Medical School, Harvard University, Cambridge (MA), USA
Aditya Apté	Department of medical physics, Memorial Sloan Kettering Cancer Center, New York (NY), USA
Saeed Ashrafinia	Department of radiology and radiological science, School of Medicine, Johns Hopkins University, Baltimore (MD), USA
Jorn Beukinga	Department of nuclear medicine and molecular imaging, University of Groningen, University Medical Center Groningen (UMCG), Groningen, the Netherlands

continued on next page

Ronald Boellaard	Department of nuclear medicine and molecular imaging, University of Groningen, University Medical Center Groningen (UMCG), Groningen, the Netherlands
Luca Boldrini	Department of radiation oncology, Gemelli ART, Università Cattolica del Sacro Cuore, Rome, Italy
Marie-Charlotte Desserroit	Laboratory of medical information processing (LaTIM)–team ACTION (image-guided therapeutic action in oncology), INSERM, UMR 1101, University of Brest, IBSAM, Brest France
Nicola Dinapoli	Department of radiation oncology, Gemelli ART, Università Cattolica del Sacro Cuore, Rome, Italy
Cuong Viet Dinh	Imaging technology for radiation therapy group, the Netherlands Cancer Institute (NKI), Amsterdam, the Netherlands
Issam El Naqa	Medical physics unit, department of oncology, McGill University, Montreal, Canada
Andriy Y. Fedorov	Surgical Planning Laboratory, Brigham and Women's Hospital and Harvard Medical School, Harvard University, Cambridge (MA), USA
Nils Gähler	Medical and biological informatics, German Cancer Research Center (DKFZ), Heidelberg, Germany
Robert Gillies	Department of cancer imaging and metabolism, Moffitt Cancer Center, Tampa (FL), USA
Michael Götz	Medical and biological informatics, German Cancer Research Center (DKFZ), Heidelberg, Germany
Matthias Guckenberger	Department of radiation oncology, University Hospital Zurich, University of Zurich, Switzerland
Mathieu Hatt	Laboratory of medical information processing (LaTIM)–team ACTION (image-guided therapeutic action in oncology), INSERM, UMR 1101, University of Brest, IBSAM, Brest France
Fabian Isensee	Medical and biological informatics, German Cancer Research Center (DKFZ), Heidelberg, Germany
Jayashree Kalpathy-Cramer	Athinoula A. Martinos Center for Biomedical Imaging, Massachusetts General Hospital (MGH) and Harvard Medical School, Harvard University, Cambridge (MA), USA
Philippe Lambin	Department of radiation oncology (MAASTRO), GROW–School for Oncology and Developmental Biology, Maastricht University Medical Centre+, Maastricht, the Netherlands
Stefan Leger	OncoRay–National Center for Radiation Research in Oncology, faculty of medicine and university hospital Carl Gustav Carus, Technische Universität Dresden, and Helmholtz-Zentrum Dresden-Rossendorf, Dresden, Germany

continued on next page

Ralph T.H. Leijenaar	Department of radiation oncology (MAASTRO), GROW–School for Oncology and Developmental Biology, Maastricht University Medical Centre+, Maastricht, the Netherlands
Jacopo Lenkowicz	Department of radiation oncology, Gemelli ART, Università Cattolica del Sacro Cuore, Rome, Italy
Fiona Lippert	Section for biomedical physics, department of radiation oncology, Universitätsklinikum Tübingen, Eberhard Karls University Tübingen, Germany
Steffen Löck	OncoRay–National Center for Radiation Research in Oncology, faculty of medicine and university hospital Carl Gustav Carus, Technische Universität Dresden, and Helmholtz-Zentrum Dresden-Rossendorf, Dresden, Germany
Are Losnegård	Department of clinical medicine, University of Bergen, Bergen, Norway
Dennis S. Mackin	Department of radiation physics, University of Texas MD Anderson Cancer Center, Houston (TX), USA
Klaus H. Maier-Hein	Medical and biological informatics, German Cancer Research Center (DKFZ), Heidelberg, Germany
Olivier Morin	Department of radiation oncology, University of California, San Francisco (CA), USA
Marta Nesteruk	Department of radiation oncology, University Hospital Zurich, University of Zurich, Switzerland
Arman Rahmim	Department of radiology and radiological science, School of Medicine, Johns Hopkins University, Baltimore (MD), USA
Arvind U.K. Rao	Department of bioinformatics and computational biology, The University of Texas MD Anderson Cancer Center, Houston (TX), USA
Christian Richter	OncoRay–National Center for Radiation Research in Oncology, faculty of medicine and university hospital Carl Gustav Carus, Technische Universität Dresden, and Helmholtz-Zentrum Dresden-Rossendorf, Dresden, Germany
Nanna M. Sijtsema	Department of radiation oncology, University of Groningen, University Medical Center Groningen (UMCG), Groningen, The Netherlands
Jairo Socarras Fernandez	Section for biomedical physics, department of radiation oncology, Universitätsklinikum Tbingen, Eberhard Karls University Tübingen, Germany
Emiliano Spezi	Biomedical engineering research group, Cardiff School of Engineering, Cardiff University, Cardiff, United Kingdom
Roel J.H.M Steenbakkers	Department of radiation oncology, University of Groningen, University Medical Center Groningen (UMCG), Groningen, The Netherlands

continued on next page

Stephanie Tanadini-Lang	Department of radiation oncology, University Hospital Zurich, University of Zurich, Switzerland
Daniela Thorwarth	Section for biomedical physics, department of radiation oncology, Universitätsklinikum Tübingen, Eberhard Karls University Tübingen, Germany
Esther Troost	OncoRay—National Center for Radiation Research in Oncology, faculty of medicine and university hospital Carl Gustav Carus, Technische Universität Dresden, and Helmholtz-Zentrum Dresden-Rossendorf, Dresden, Germany
Taman Upadhyaya	Laboratory of medical information processing (LaTIM)—team ACTION (image-guided therapeutic action in oncology), INSERM, UMR 1101, University of Brest, IBSAM, Brest France
Vincenzo Valentini	Department of radiation oncology, Gemelli ART, Università Cattolica del Sacro Cuore, Rome, Italy
Martin Vallières	Medical physics unit, McGill University, Montreal, Canada
Ulke van der Heide	Imaging technology for radiation therapy group, the Netherlands Cancer Institute (NKI), Amsterdam, the Netherlands
Lisanne V. van Dijk	Department of radiation oncology, University of Groningen, University Medical Center Groningen (UMCG), Groningen, The Netherlands
Floris H.P. van Velden	Department of radiology, Leiden University Medical Center (LUMC), Leiden, the Netherlands
Joost van Griethuysen	Department of radiology, the Netherlands Cancer Institute (NKI), Amsterdam, the Netherlands
Philip Whybra	Biomedical engineering research group, Cardiff School of Engineering, Cardiff University, Cardiff, United Kingdom
Alex Zwanenburg	National Center for Tumor Diseases (NCT), partner site Dresden, Germany

Table 1: Alphabetical list of IBSI collaborators.

Contents

1	On this document	1
1.1	Changes	1
2	Imaging features	3
2.1	Morphological features	3
2.1.1	Volume	4
2.1.2	Approximate volume	5
2.1.3	Surface area	5
2.1.4	Surface to volume ratio	5
2.1.5	Compactness 1	6
2.1.6	Compactness 2	6
2.1.7	Spherical disproportion	6
2.1.8	Sphericity	6
2.1.9	Asphericity	6
2.1.10	Centre of mass shift	7
2.1.11	Maximum 3D diameter	7
2.1.12	Major axis length	7
2.1.13	Minor axis length	8
2.1.14	Least axis length	8
2.1.15	Elongation	8
2.1.16	Flatness	8
2.1.17	Volume density - axis-aligned bounding box	8
2.1.18	Area density - axis-aligned bounding box	9
2.1.19	Volume density - oriented minimum bounding box	9
2.1.20	Area density - oriented minimum bounding box	9
2.1.21	Volume density - approximate enclosing ellipsoid	9
2.1.22	Area density - approximate enclosing ellipsoid	9
2.1.23	Volume density - minimum volume enclosing ellipsoid	10
2.1.24	Area density - minimum volume enclosing ellipsoid	10
2.1.25	Volume density - convex hull	10
2.1.26	Area density - convex hull	10
2.1.27	Integrated intensity	11
2.1.28	Moran's I index	11
2.1.29	Geary's C measure	11
2.2	Local intensity features	11
2.2.1	Local intensity peak	11
2.2.2	Global intensity peak	12

2.3	Statistical features	12
2.3.1	Mean	12
2.3.2	Variance	12
2.3.3	Skewness	12
2.3.4	Kurtosis	13
2.3.5	Median	13
2.3.6	Minimum grey level	13
2.3.7	10 th percentile	13
2.3.8	90 th percentile	13
2.3.9	Maximum grey level	13
2.3.10	Interquartile range	13
2.3.11	Range	13
2.3.12	Mean absolute deviation	14
2.3.13	Robust mean absolute deviation	14
2.3.14	Median absolute deviation	14
2.3.15	Coefficient of variation	14
2.3.16	Quartile coefficient of dispersion	14
2.3.17	Energy	15
2.3.18	Root mean square	15
2.4	Intensity histogram features	15
2.4.1	Intensity histogram mean	15
2.4.2	Intensity histogram variance	15
2.4.3	Intensity histogram skewness	16
2.4.4	Intensity histogram kurtosis	16
2.4.5	Intensity histogram median	16
2.4.6	Intensity histogram minimum grey level	16
2.4.7	Intensity histogram 10 th percentile	16
2.4.8	Intensity histogram 90 th percentile	17
2.4.9	Intensity histogram maximum grey level	17
2.4.10	Intensity histogram mode	17
2.4.11	Intensity histogram interquartile range	17
2.4.12	Intensity histogram range	17
2.4.13	Intensity histogram mean absolute deviation	17
2.4.14	Intensity histogram robust mean absolute deviation	17
2.4.15	Intensity histogram median absolute deviation	18
2.4.16	Intensity histogram coefficient of variation	18
2.4.17	Intensity histogram quartile coefficient of dispersion	18
2.4.18	Intensity histogram entropy	18
2.4.19	Intensity histogram uniformity	18
2.4.20	Maximum histogram gradient	19
2.4.21	Maximum histogram gradient grey level	19
2.4.22	Minimum histogram gradient	19
2.4.23	Minimum histogram gradient grey level	19
2.5	Intensity-volume histogram features	19
2.5.1	Volume at intensity fraction	20
2.5.2	Intensity at volume fraction	21
2.5.3	Volume at intensity fraction difference	21
2.5.4	Intensity at volume fraction difference	21
2.5.5	Area under IVH curve	21

2.6	Textural features - Grey level co-occurrence based features	21
2.6.1	Joint maximum	23
2.6.2	Joint average	23
2.6.3	Joint variance	23
2.6.4	Joint entropy	24
2.6.5	Difference average	24
2.6.6	Difference variance	25
2.6.7	Difference entropy	25
2.6.8	Sum average	26
2.6.9	Sum variance	26
2.6.10	Sum entropy	26
2.6.11	Angular second moment	26
2.6.12	Contrast	26
2.6.13	Dissimilarity	26
2.6.14	Inverse difference	27
2.6.15	Inverse difference normalised	27
2.6.16	Inverse difference moment	27
2.6.17	Inverse difference moment normalised	27
2.6.18	Inverse variance	27
2.6.19	Correlation	27
2.6.20	Autocorrelation	28
2.6.21	Cluster tendency	28
2.6.22	Cluster shade	28
2.6.23	Cluster prominence	29
2.6.24	First measure of information correlation	29
2.6.25	Second measure of information correlation	29
2.7	Textural features - Grey level run length based features	29
2.7.1	Short runs emphasis	30
2.7.2	Long runs emphasis	30
2.7.3	Low grey level run emphasis	30
2.7.4	High grey level run emphasis	30
2.7.5	Short run low grey level emphasis	31
2.7.6	Short run high grey level emphasis	31
2.7.7	Long run low grey level emphasis	32
2.7.8	Long run high grey level emphasis	32
2.7.9	Grey level non-uniformity	32
2.7.10	Grey level non-uniformity normalised	32
2.7.11	Run length non-uniformity	32
2.7.12	Run length non-uniformity normalised	32
2.7.13	Run percentage	33
2.7.14	Grey level variance	33
2.7.15	Run length variance	33
2.7.16	Run entropy	33
2.8	Textural features - Grey level size zone based features	33
2.8.1	Small zone emphasis	34
2.8.2	Large zone emphasis	34
2.8.3	Low grey level zone emphasis	35
2.8.4	High grey level zone emphasis	35
2.8.5	Small zone low grey level emphasis	35

2.8.6	Small zone high grey level emphasis	36
2.8.7	Large zone low grey level emphasis	36
2.8.8	Large zone high grey level emphasis	36
2.8.9	Grey level non-uniformity	36
2.8.10	Grey level non-uniformity normalised	36
2.8.11	Zone size non-uniformity	36
2.8.12	Zone size non-uniformity normalised	37
2.8.13	Zone percentage	37
2.8.14	Grey level variance	37
2.8.15	Zone size variance	37
2.8.16	Zone size entropy	37
2.9	Textural features - Neighbourhood grey tone difference based features	37
2.9.1	Coarseness	38
2.9.2	Contrast	39
2.9.3	Busyness	39
2.9.4	Complexity	40
2.9.5	Strength	40
2.10	Textural features - Grey level distance zone based features	40
2.10.1	Small distance emphasis	41
2.10.2	Large distance emphasis	42
2.10.3	Low grey level zone emphasis	42
2.10.4	High grey level zone emphasis	42
2.10.5	Small distance low grey level emphasis	42
2.10.6	Small distance high grey level emphasis	42
2.10.7	Large distance low grey level emphasis	42
2.10.8	Large distance high grey level emphasis	43
2.10.9	Grey level non-uniformity	43
2.10.10	Grey level non-uniformity normalised	43
2.10.11	Zone distance non-uniformity	43
2.10.12	Zone distance non-uniformity normalised	43
2.10.13	Zone percentage	43
2.10.14	Grey level variance	44
2.10.15	Zone distance variance	44
2.10.16	Zone distance entropy	44
2.11	Textural features - Neighbouring grey level dependence based features	44
2.11.1	Low dependence emphasis	45
2.11.2	High dependence emphasis	46
2.11.3	Low grey level count emphasis	46
2.11.4	High grey level count emphasis	46
2.11.5	Low dependence low grey level emphasis	46
2.11.6	Low dependence high grey level emphasis	46
2.11.7	High dependence low grey level emphasis	46
2.11.8	High dependence high grey level emphasis	47
2.11.9	Grey level non-uniformity	47
2.11.10	Grey level non-uniformity normalised	47
2.11.11	Dependence count non-uniformity	47
2.11.12	Dependence count non-uniformity normalised	47
2.11.13	Dependence count percentage	47
2.11.14	Grey level variance	48

<i>CONTENTS</i>	ix
2.11.15 Dependence count variance	48
2.11.16 Dependence count entropy	48
2.11.17 Dependence count energy	48

Chapter 1

On this document

While analysis of medical images has practically taken place since the first image was recorded, high throughput analysis of medical images is a more recent phenomenon (Kumar et al., 2012; Lambin et al., 2012; Gillies et al., 2015). The aim of such a radiomics process is to provide decision support based on medical imaging. Part of the radiomics process is the conversion of image data into numerical features which capture different medical image aspects, and can be subsequently correlated as biomarkers to e.g. expected oncological treatment outcome.

With the growth of the radiomics field, it has become clear that results are often difficult to reproduce, that standards for image processing and feature extraction are missing, and that reporting guidelines are absent (Gillies et al., 2015; Hatt et al., 2015; Yip and Aerts, 2016). The image biomarker standardisation initiative (IBSI) seeks to address these issues. The current document provides definitions for a large number of image features.

While the definitions contained in the document have been checked and tested, errors may occur. Should you encounter an error, unclear descriptions, missing references, etc., please contact us to make the necessary changes.

The definitions presented in the document may furthermore contain references to digital phantoms and other test data. These are used by IBSI to standardise feature implementations and image processing schemes. These data sets and corresponding standardised feature values will be made publicly available at a later time point.

1.1 Changes

New versions of the document include improvements and additions. The following is a list of the changes made in each version:

Version 1.3

- Updated and revised definitions of morphological features to handle inconsistencies due to mixed voxel representations. Notably *volume* is now calculated from the ROI mesh instead of directly from the ROI voxels. Likewise, *diameter*, *volume density* and *area density* features are (where possible) based on vertices of the ROI mesh, instead of the voxel centre point set. The introductory description of the morphological feature set was updated to introduce nomenclature and definitions used in meshes.
- Added *approximate volume* feature, which captures tumour volume based on voxel counts.

- Added figures to show feature calculation process for texture features.
- Clarified definitions for *Neighbourhood grey tone difference matrix*-based features.

Version 1.2

- Updated the section on *Intensity volume histogram*-based features.
- Updated description for the local intensity feature set.
- Updated the description of the *area density - approximate enclosing ellipsoid* to provide a maximum degree for the Legendre polynomials.
- Updated the description of the *volume density - minimum volume enclosing ellipsoid* to provide a stopping tolerance for Khachiyan's method.
- Feature sets are ordered differently. The morphological features are now presented first, followed by local intensity features and statistical features.
- Fixed various typos.

Version 1.1

- Fixed errors in the definition of *dependence count energy* feature.
- Fixed errors in the definitions of *major axis length*, *minor axis length* and *least axis length* features.
- Updated descriptions of the *volume density - approximate enclosing ellipsoid* and *area density - approximate enclosing ellipsoid* features.
- Added descriptions of the *volume density - minimum volume enclosing ellipsoid* and *area density - minimum volume enclosing ellipsoid* features.
- Fixed errors in layout.

Chapter 2

Imaging features

In this chapter we will describe a set of quantitative imaging features. The set of features largely builds upon the feature sets proposed by Aerts et al. (2014) and Hatt et al. (2016), and will be described in full. The set of features can be divided into a number of families, of which statistical, intensity histogram-based, intensity-volume histogram-based, morphological features, local intensity, and textural features are treated here. The feature set described here is necessarily incomplete, yet should cover most of the commonly used features.

Features are calculated on the base image, as well as its filter reconstructions. It is assumed that an image segmentation map, identifying the voxels corresponding to the region of interest (ROI), exists.

The required image processing steps before feature calculation depends on the particular feature family. Several feature families require prior discretisation of grey levels into grey level bins, notably intensity histogram and textural features. The other feature families do not require discretisation before calculations.

2.1 Morphological features

Morphological features describe geometric aspects of a region of interest (ROI), such as area and volume. Morphological features are based on ROI voxel representations of the volume. Three voxel representations of the volume are conceivable. First, the volume can be represented by a stack of voxels with each taking up a certain volume. Second, the voxel point set \mathbf{X}_c consisting of coordinates of the voxel centers may be used. The third option is representation of the outer structure of the volume by mesh vertices and faces. We use the second representation when the inner structure of the volume is important, and the third representation when only the outer surface structure is important. The first representation is not used because it does not deal with partial volume effects, and to avoid inconsistencies introduced by mixing representations in small voxel volumes.

Mesh-based representation The surface of the ROI volume can be translated into a triangle mesh using a meshing algorithm. While there are multiple meshing algorithms available, we suggest the use of the *Marching Cubes* algorithm (Lorensen and Cline, 1987; Lewiner et al., 2003) because of its widespread availability for different programming languages and reasonable approximation of the surface area and volume (Stelldinger et al., 2007). In practice, mesh-derived feature values depend upon the meshing algorithm used and small differences may occur.

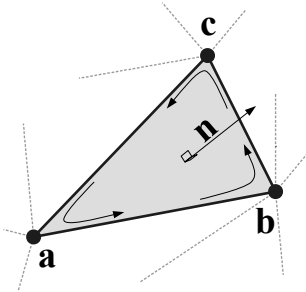


Figure 2.1: Meshing algorithms draw faces and vertices to cover the ROI. One face, spanned by vertices \mathbf{a} , \mathbf{b} and \mathbf{c} , is highlighted. Moreover, the vertices define the three edges $\mathbf{ab} = \mathbf{b} - \mathbf{a}$, $\mathbf{bc} = \mathbf{c} - \mathbf{b}$ and $\mathbf{ca} = \mathbf{a} - \mathbf{c}$. The face normal \mathbf{n} is determined using the right-hand rule, and calculated as $\mathbf{n} = (\mathbf{ab} \times \mathbf{bc}) / \|\mathbf{ab} \times \mathbf{bc}\|$, i.e. the outer product of edge \mathbf{ab} with edge \mathbf{bc} , normalised by its length.

Meshing algorithms use the ROI voxel point set \mathbf{X}_c to create a closed mesh. Dependent on the algorithm, a parameter is required to specify where the mesh should be drawn. A default level of 0.5 times the voxel spacing is used for marching cube algorithms. Alternatively a value of 0.5 can be used for isosurface algorithms, when the ROI mask consists of 0 and 1 values. Depending on implementation, isosurface algorithms may also require padding of the ROI mask with non-ROI voxels to correctly estimate the isosurface contours in places where ROI voxels would otherwise be located at the edge of the mask.

The closed mesh drawn by the meshing algorithm consists of N_{fc} triangle faces spanned by N_{vx} vertex points, see Figure 2.1. The set of vertex points is then \mathbf{X}_{vx} .

The calculation of the mesh volume requires that all faces have the same orientation of the face normal. Consistent orientation can be checked by the fact that in a regular, closed mesh, all edges are shared between exactly two faces. Given the edge spanned by vertices \mathbf{a} and \mathbf{b} , the edge must be $\mathbf{ab} = \mathbf{b} - \mathbf{a}$ for one face and $\mathbf{ba} = \mathbf{a} - \mathbf{b}$ for the adjacent faces. This ensures consistent application of the right-hand rule, and thus consistent orientation of the face normals. Algorithm implementations may return consistently orientated faces by default.

Missing internal voxels The ROI may enclose one or more volumes of missing voxels, as with the test volume. Whereas most other features would not assess the voxels contained in these volumes at all, in the case of morphological features such voxels may be included. For example, voxels may be omitted due to having grey levels outside of a prescribed range. The resulting volumes may be very small and carry no physiological meaning. From a morphological perspective, it then makes sense that these voxels are included for the calculation of morphological features. The volume threshold for inclusion of internal volumes depends on the particular situation, and should be reported.

The missing interior voxel in the digital phantom should be considered as an external volume for the calculation of morphological features.

2.1.1 Volume

The volume V is calculated from the ROI mesh as follows (Zhang and Chen, 2001). Each face can be viewed as forming a tetrahedron with the origin as the remaining vertex. By placing the

origin at $(0, 0, 0)$, the signed volume of each tetrahedron formed by face k and the origin is:

$$V_k = \frac{\mathbf{a} \cdot (\mathbf{b} \times \mathbf{c})}{6}$$

Here \mathbf{a} , \mathbf{b} and \mathbf{c} are the vertex points of face k . Depending on the orientation of the normal, the signed volume may be positive or negative. Hence, the orientation of face normals should be consistent, e.g. all normals must be either pointing 'outward' or 'inward'. The volume V is then calculated by summing over the face volumes, and taking the absolute value:

$$V = \left| \sum_{k=1}^{N_{fc}} V_k \right|$$

For positron emission tomography *volume* is equivalent to the *metabolically active tumour volume* (MATV).

2.1.2 Approximate volume

In clinical practice, volumes are commonly determined on voxel counts. For larger volumes, the differences between *approximate volume* and mesh-based volume are usually negligible. However for small volumes with a low number of voxels *approximate volume* will overestimate volume compared to mesh-based volume. It is therefore only used as a reference feature, and not in the calculation of other morphological features.

Approximate volume is defined as:

$$F_{morph.approx.vol} = \sum_{j=1}^{N_v} V_j$$

Here N_v is the number of voxels in the ROI, and V_j the volume of voxel j .

2.1.3 Surface area

The area A is also calculated from the ROI mesh, by summing over the face area surfaces. The area of face k is then:

$$A_k = \frac{|\mathbf{ab} \times \mathbf{ac}|}{2}$$

Here $\mathbf{ab} = \mathbf{b} - \mathbf{a}$ is the vector from vertex \mathbf{a} to vertex \mathbf{b} , and $\mathbf{ac} = \mathbf{c} - \mathbf{a}$ the vector from vertex \mathbf{a} to vertex \mathbf{c} . The total surface area A is then:

$$A = \sum_{k=1}^{N_{fc}} A_k$$

2.1.4 Surface to volume ratio

The surface to volume ratio is given as:

$$F_{morph.av} = \frac{A}{V}$$

2.1.5 Compactness 1

The following are several features describing the deviation of the ROI volume from a sphere. All these definitions can be derived from one another. As a results these features are are highly correlated and may thus redundant. Compactness 1 is a measure for how compact, or sphere-like the volume is. Compactness 1 is defined as:

$$F_{morph.comp.1} = \frac{V}{\pi^{1/2} A^{3/2}}$$

Some definitions use $A^{2/3}$ instead of $A^{3/2}$, e.g. (Aerts et al., 2014). This is most likely an error, as the feature would no longer be dimensionless.

2.1.6 Compactness 2

Compactness 2 is another measure to describe how sphere-like the volume is:

$$F_{morph.comp.2} = 36\pi \frac{V^2}{A^3}$$

By definition $F_{morph.comp.1} = 1/6\pi (F_{morph.comp.2})^{1/2}$.

2.1.7 Spherical disproportion

Spherical disproportion is another measure to describe how sphere-like the volume is:

$$F_{morph.sph.dispr} = \frac{A}{4\pi R^2} = \frac{A}{(36\pi V^2)^{1/3}}$$

By definition $F_{morph.sph.dispr} = (F_{morph.comp.2})^{-1/3}$.

2.1.8 Sphericity

Sphericity is a further measure to describe how sphere-like the volume is:

$$F_{morph.sphericity} = \frac{(36\pi V^2)^{1/3}}{A}$$

By definition $F_{morph.sphericity} = (F_{morph.comp.2})^{1/3}$.

2.1.9 Asphericity

Asphericity describes how much the ROI deviates from a perfect sphere. Asphericity is defined as:

$$F_{morph.asphericity} = \left(\frac{1}{36\pi} \frac{A^3}{V^2} \right)^{1/3} - 1$$

By definition $F_{morph.asphericity} = (F_{morph.comp.2})^{-1/3} - 1$

2.1.10 Centre of mass shift

The distance between the ROI volume centroid and the intensity-weighted ROI volume centroid measures the placement of high and low intensity regions within the volume. The ROI volume centre of mass is calculated from the ROI voxel point set \mathbf{X}_c as follows:

$$\overrightarrow{CoM}_{geom} = \frac{1}{N_v} \sum_{i=1}^{N_v} \vec{X}_{c,i}$$

For the intensity-weighted ROI volume centre of mass each voxel centre in \mathbf{X}_c is weighted by its intensity using the corresponding grey level in \mathbf{X}_{gl} :

$$\overrightarrow{CoM}_{gl} = \frac{\sum_{i=1}^{N_v} X_{gl,i} \vec{X}_{c,i}}{\sum_{i=1}^{N_v} X_{gl,i}}$$

The distance between the two centres of mass is then:

$$F_{morph.com} = \|\overrightarrow{CoM}_{geom} - \overrightarrow{CoM}_{gl}\|_2$$

2.1.11 Maximum 3D diameter

The maximum 3D diameter is the distance between the two most distant vertices in the ROI mesh vertex set \mathbf{X}_{vx} :

$$F_{morph.diam} = \max \left(\|\vec{X}_{vx,i} - \vec{X}_{vx,j}\|_2 \right), \quad i = 1, \dots, N \quad j = 1, \dots, N$$

A practical way of determining the maximum 3D diameter is to first construct the convex hull of the ROI mesh. The convex hull vertex set $\mathbf{X}_{vx,convex}$ is guaranteed to contain the two most distant vertices of \mathbf{X}_{vx} . This significantly reduces the computational cost of calculating distance between all vertices. Despite the remaining $O(n^2)$ cost of calculating distances between different vertices, the size of $\mathbf{X}_{vx,convex}$ is usually considerably smaller than the size of \mathbf{X}_{vx} . Moreover, the convex hull is later used for the calculation of other morphological features.

2.1.12 Major axis length

Principal component analysis (PCA) can be used to determine the main orientation of the ROI. On a three dimensional object, PCA yields three orthogonal eigenvectors $\{e_1, e_2, e_3\}$ and three eigenvalues $(\lambda_1, \lambda_2, \lambda_3)$. These eigenvalues and eigenvectors geometrically describe a triaxial ellipsoid. The three eigenvectors determine the orientation of the ellipsoid, whereas the eigenvalues provide a measure of how far the ellipsoid extends along each eigenvector.

The eigenvalues can be ordered so that $\lambda_{major} \geq \lambda_{minor} \geq \lambda_{least}$ correspond to the major, minor and least axes of the ellipsoid respectively. The semi-axes lengths a , b and c for the major, minor and least axes are then $2\sqrt{\lambda_{major}}$, $2\sqrt{\lambda_{minor}}$ and $2\sqrt{\lambda_{least}}$ respectively. The major axis length is twice the semi-axis length a , determined using the largest eigenvalue obtained by PCA on the point set of voxel centers \mathbf{X}_c (Heiberger and Holland, 2015):

$$F_{morph.pca.major} = 2a = 4\sqrt{\lambda_{major}}$$

2.1.13 Minor axis length

The minor axis length of the ROI provides a measure of how far the volume extends along the second largest axis. The minor axis length is twice the semi-axis length b , determined using the second largest eigenvalue obtained by PCA on the point set of voxel centers \mathbf{X}_c (Heiberger and Holland, 2015):

$$F_{morph.pca.minor} = 2b = 4\sqrt{\lambda_{minor}}$$

2.1.14 Least axis length

The least axis is the axis along which the object is least extended. The least axis length is twice the semi-axis length c , determined using the smallest eigenvalue obtained by PCA on the point set of voxel centers \mathbf{X}_c (Heiberger and Holland, 2015):

$$F_{morph.pca.least} = 2c = 4\sqrt{\lambda_{least}}$$

2.1.15 Elongation

The ratio of the major and minor axis lengths could be viewed as the extent to which a volume is longer than it is wide, i.e. is eccentric. For computational reasons, we express elongation as an inverse ratio. 1 is thus completely non-elongated, e.g. a sphere, and smaller values express greater elongation of the ROI volume.

$$F_{morph.pca.elongation} = \sqrt{\frac{\lambda_{minor}}{\lambda_{major}}}$$

2.1.16 Flatness

The ratio of the major and least axis lengths could be viewed as the extent to which a volume is flat relative to its length. For computational reasons, we express flatness as an inverse ratio. 1 is thus completely non-flat, e.g. a sphere, and smaller values express objects which are increasingly flatter.

$$F_{morph.pca.flatness} = \sqrt{\frac{\lambda_{least}}{\lambda_{major}}}$$

2.1.17 Volume density - axis-aligned bounding box

Volume density is the fraction of the ROI volume and a comparison volume. Here the comparison volume is that of the axis-aligned bounding box of the ROI mesh vertex set \mathbf{X}_{vx} or the ROI mesh convex hull vertex set $\mathbf{X}_{vx,convex}$. Both vertex sets generate an identical bounding box, which is the smallest box enclosing the vertex set, and aligned with the axes of the reference frame. Thus:

$$F_{morph.v.dens.aabb} = \frac{V}{V_{aabb}}$$

This feature is also called *extent* (El Naqa et al., 2009).

2.1.18 Area density - axis-aligned bounding box

Conceptually similar to the *volume density - axis-aligned bounding box* feature, *area density* considers the ratio of the ROI surface area and the surface area A_{aabb} of the axis-aligned bounding box enclosing the ROI mesh vertex set \mathbf{X}_{vx} (van Dijk et al., 2016). The bounding box is identical to the one used in the *volume density - axis-aligned bounding box* feature. Thus:

$$F_{morph.a.dens.aabb} = \frac{A}{A_{aabb}}$$

2.1.19 Volume density - oriented minimum bounding box

The volume of an axis-aligned bounding box is generally not the smallest obtainable volume enclosing the ROI. By orienting the box along a different set of axes, a smaller enclosing volume may be attainable. The oriented minimum bounding box of the ROI mesh vertex set \mathbf{X}_{vx} or $\mathbf{X}_{vx,convex}$ encloses the vertex set and has the smallest possible volume. A 3-dimensional rotating callipers technique was devised by O'Rourke (1985) to derive the oriented minimum bounding box. Due to computational complexity of the rotating callipers technique, the oriented minimum bounding box is commonly approximated at lower complexity, see e.g. Barequet and Har-Peled (2001) and Chan and Tan (2001). Thus:

$$F_{morph.v.dens.ombb} = \frac{V}{V_{ombb}}$$

Here V_{ombb} is the volume of the oriented minimum bounding box.

2.1.20 Area density - oriented minimum bounding box

The area density is estimated as:

$$F_{morph.a.dens.ombb} = \frac{A}{A_{ombb}}$$

Here A_{ombb} is the surface area of the same bounding box as calculated for the *volume density - oriented minimum bounding box* feature.

2.1.21 Volume density - approximate enclosing ellipsoid

The eigenvectors and eigenvalues from principal component analysis of the ROI voxel center point set \mathbf{X}_c can be used to describe an ellipsoid approximating the point cloud (Mazurowski et al., 2016). The volume of an ellipsoid is $V_{aee} = 4\pi a b c / 3$, with a , b , and c being the length of the ellipsoid's semi-principal axes (Weisstein, 2016), see section 2.1.12. The volume density is then:

$$F_{morph.v.dens.aee} = \frac{3V}{4\pi abc}$$

2.1.22 Area density - approximate enclosing ellipsoid

The surface area of an ellipsoid can generally not be evaluated in an elementary form. However, it is possible to approximate the surface using a infinite series. We use the same semi-principal axes as for the *volume density - approximate ellipsoid* feature and define:

$$A_{aee}(a, b, c) = 4\pi a b \sum_{\nu=0}^{\infty} \frac{(\alpha \beta)^\nu}{1 - 4\nu^2} P_\nu \left(\frac{\alpha^2 + \beta^2}{2\alpha\beta} \right)$$

Here $\alpha = \sqrt{1 - b^2/a^2}$ and $\beta = \sqrt{1 - c^2/a^2}$ are eccentricities of the ellipsoid and P_ν is the Legendre polynomial function for degree ν . Though infinite, the series converges, and calculation may be stopped early. Gains in precision past $\nu = 20$ are very limited, and as a default we stop calculations at this polynomial degree.

The area density is then approximately:

$$F_{morph.a.dens.aee} = \frac{A}{A_{aee}}$$

2.1.23 Volume density - minimum volume enclosing ellipsoid

The *approximate ellipsoid* may not enclose the ROI or be the smallest enclosing ellipsoid. The minimum volume enclosing ellipsoid is generally approximated to make calculation more feasible. Various algorithms have been described, e.g. (Todd and Yldrm, 2007; Ahipaolu, 2015), which are usually elaborations on Khachiyan's barycentric coordinate descent method (Khachiyan, 1996).

The minimum volume enclosing ellipsoid encloses the ROI mesh vertex set \mathbf{X}_{vx} or $\mathbf{X}_{vx,convex}$. The volume of the minimum volume enclosing ellipsoid is defined by its semi-axes lengths $V_{mvee} = 4\pi a b c / 3$. Then:

$$F_{morph.v.dens.mvee} = \frac{V}{V_{mvee}}$$

For Khachiyan's barycentric coordinate descent-based methods we use a default tolerance $\tau = 0.001$ as stopping criterion.

2.1.24 Area density - minimum volume enclosing ellipsoid

The surface area of an ellipsoid does not have a general elementary form, but should be approximated, see section 2.1.22. Let the approximated surface area be A_{mvee} . Then:

$$F_{morph.a.dens.mvee} = \frac{A}{A_{mvee}}$$

2.1.25 Volume density - convex hull

The convex hull encloses ROI mesh vertex set \mathbf{X}_{vx} and consists of the vertex set $\mathbf{X}_{vx,convex}$ and corresponding faces. The volume of the ROI mesh convex hull set is calculated as for the *volume* feature. The volume density can then be calculated as follows:

$$F_{morph.v.dens.conv.hull} = \frac{V}{V_{convex}}$$

This feature is also called *solidity* (El Naqa et al., 2009).

2.1.26 Area density - convex hull

The area of the convex hull is the sum of the area of the faces of the convex hull, as in the calculation of the *area* feature. The convex hull is identical to the one used in the *volume density - convex hull* feature. Then:

$$F_{morph.a.dens.conv.hull} = \frac{A}{A_{convex}}$$

2.1.27 Integrated intensity

Integrated intensity is the average grey level multiplied by the volume. In the context of ^{18}F -FDG-PET, this feature is called *total legion glycolysis* (Vaidya et al., 2012). Thus:

$$F_{morph.integ.int} = V \frac{1}{N_v} \sum_{i=1}^{N_v} X_{gl,i}$$

2.1.28 Moran's I index

Moran's I index is an indicator of spatial autocorrelation (Moran, 1950; Dale et al., 2002). It is defined as:

$$F_{morph.moran.i} = \frac{N_v}{\sum_{i=1}^{N_v} \sum_{j=1}^{N_v} w_{ij}} \frac{\sum_{i=1}^{N_v} \sum_{j=1}^{N_v} w_{ij} (X_{gl,i} - \mu) (X_{gl,j} - \mu)}{\sum_{i=1}^{N_v} (X_{gl,i} - \mu)^2}, \quad i \neq j$$

μ is the mean of \mathbf{X}_{gl} and w_{ij} is a weight factor, equal to the inverse Euclidean distance between voxels i and j of the ROI voxel point set \mathbf{X}_c (Da Silva et al., 2008). Moran's index values close to 1.0, 0.0 and -1.0 indicate high spatial autocorrelation, no spatial autocorrelation and high spatial anti-autocorrelation respectively.

2.1.29 Geary's C measure

Geary's C measures spatial autocorrelation, like Moran's I index (Geary, 1954; Dale et al., 2002). Geary's C however, directly measures grey level differences between voxels and is more sensitive to local spatial autocorrelation. This measure is defined as:

$$F_{morph.geary.c} = \frac{N_v - 1}{2 \sum_{i=1}^{N_v} \sum_{j=1}^{N_v} w_{ij}} \frac{\sum_{i=1}^{N_v} \sum_{j=1}^{N_v} w_{ij} (X_{gl,i} - X_{gl,j})^2}{\sum_{i=1}^{N_v} (X_{gl,i} - \mu)^2}, \quad i \neq j$$

As with Moran's I , μ is the mean of \mathbf{X}_{gl} and w_{ij} is a weight factor, equal to the inverse Euclidean distance between voxels i and j of the ROI voxel point set \mathbf{X}_c (Da Silva et al., 2008).

2.2 Local intensity features

Local intensity features are a feature set where grey levels within a defined neighbourhood around a centre voxel are considered. The grey levels in the neighbourhood are subsequently summarised. Unlike many feature sets, local features require the image and ROI mapping separately. While local intensity features are calculated for voxels within the ROI, the complete image is used to define the local neighbourhoods. This means that for these features the image and ROI should not be merged by replacing image voxels outside the ROI with placeholder values.

2.2.1 Local intensity peak

The local intensity peak was originally devised for reducing variance in determining standardised uptake values (Wahl et al., 2009). It is defined as the mean grey level in a 1 cm^3 spherical volume, centered on the ROI voxel with the maximum grey level.

To calculate $F_{loc.peak.loc}$, we first select all the voxels with voxel centers within radius $r = (\frac{3}{4\pi})^{1/3} \approx 0.62 \text{ cm}$ of the voxel with the maximum grey level. Subsequently, the mean grey level of the selected voxels, including the centre voxel, are calculated.

In case the maximum grey level is found in multiple ROI voxels, *local intensity peak* is calculated for each of these voxels, and the highest local intensity peak chosen.

2.2.2 Global intensity peak

The *global intensity peak* is similar to $F_{loc.peak.loc}$. Instead of calculating an intensity peak for the voxel(s) with the maximum grey level, intensity peaks are calculated for every voxel in the ROI. The highest intensity peak value is then selected.

2.3 Statistical features

The statistical features describe how grey levels within the region of interest (ROI) are distributed. The features in this set do not require discretisation, and may be used to describe a continuous distribution, such as FDG-PET. Then, $\mathbf{X}_{gl} = \{X_{gl,1}, X_{gl,2}, \dots, X_{gl,N_v}\}$ be the set of grey levels of the N_v voxels in the ROI.

Summarising features While assessment of the entire ROI is both the assumed and preferred option, in some cases a 2 dimensional approach may be required. For example, spatial image filtering may be applied per slice instead of the entire volume in cases of large slice thickness relative to planar dimensions. Spatial filtering changes grey level values and a consistent meaning of grey levels may be lost if filtering is performed per slice. If a 2 dimensional approach is unavoidable, calculation of features per slice and subsequent averaging is recommended.

2.3.1 Mean

The mean grey level of \mathbf{X}_{gl} is calculated as:

$$F_{stat.mean} = \frac{1}{N_v} \sum_{j=1}^{N_v} X_{gl,j}$$

2.3.2 Variance

The grey level variance of \mathbf{X}_{gl} is defined as:

$$F_{stat.var} = \frac{1}{N_v} \sum_{j=1}^{N_v} (X_{gl,j} - \mu)^2$$

2.3.3 Skewness

The skewness of the grey level distribution of \mathbf{X}_{gl} is defined as:

$$F_{stat.skew} = \frac{\frac{1}{N_v} \sum_{j=1}^{N_v} (X_{gl,j} - \mu)^3}{\left(\frac{1}{N_v} \sum_{j=1}^{N_v} (X_{gl,j} - \mu)^2 \right)^{3/2}}$$

Here $\mu = F_{stat.mean}$. If the grey level variance $F_{stat.var} = 0$, $F_{stat.skew} = 0$.

2.3.4 Kurtosis

Kurtosis, or technically excess kurtosis, is calculated as measure of peakedness in the grey level distribution of \mathbf{X}_{gl} :

$$F_{stat.kurt} = \frac{\frac{1}{N_v} \sum_{j=1}^{N_v} (X_{gl,j} - \mu)^4}{\left(\frac{1}{N_v} \sum_{j=1}^{N_v} (X_{gl,j} - \mu)^2\right)^2} - 3$$

Here $\mu = F_{stat.mean}$. Note that kurtosis is corrected by a Fisher correction of -3 to center kurtosis on 0 for normal distributions. If the grey level variance $F_{stat.var} = 0$, $F_{stat.kurt} = 0$.

2.3.5 Median

The median value $F_{stat.median}$ is the sample median of \mathbf{X}_{gl} .

2.3.6 Minimum grey level

The minimum grey level is equal to the lowest grey level present in \mathbf{X}_{gl} .

2.3.7 10th percentile

P_{10} is the 10th percentile of \mathbf{X}_{gl} . P_{10} is more robust to outliers in grey level then the minimum grey level.

2.3.8 90th percentile

P_{90} is the 90th percentile of \mathbf{X}_{gl} . P_{90} is more robust to outliers in grey level then the maximum grey level.

2.3.9 Maximum grey level

The maximum grey level is equal to the highest grey level present in \mathbf{X}_{gl} .

2.3.10 Interquartile range

The interquartile range (IQR) of \mathbf{X}_{gl} is defined as:

$$F_{stat.iqr} = P_{75} - P_{25}$$

P_{25} and P_{75} are the 25th and 75th percentile of \mathbf{X}_{gl} , respectively.

2.3.11 Range

The range of grey levels is defined as:

$$F_{stat.range} = \max(\mathbf{X}_{gl}) - \min(\mathbf{X}_{gl})$$

2.3.12 Mean absolute deviation

The mean absolute deviation is a measure of dispersion from the mean of \mathbf{X}_{gl} :

$$F_{stat.mad} = \frac{1}{N_v} \sum_{j=1}^{N_v} |X_{gl,j} - \mu|$$

Here $\mu = F_{stat.mean}$.

2.3.13 Robust mean absolute deviation

The mean absolute deviation can be influenced by outliers, and mean dispersion from the mean could be affected as a consequence. The set of grey levels can be restricted to grey levels which lie closer to the center of the distribution. Let

$$\mathbf{X}_{10-90} = \{x \in \mathbf{X}_{gl} \mid P_{10}(\mathbf{X}_{gl}) \leq x \leq P_{90}(\mathbf{X}_{gl})\}$$

This means that \mathbf{X}_{10-90} is the set of $N_{10-90} \leq N$ voxels in \mathbf{X}_{gl} whose grey levels are equal to, or lie between, the values corresponding to the 10th and 90th percentiles of \mathbf{X}_{gl} . The robust mean absolute deviation is then:

$$F_{stat.rmad} = \frac{1}{N_{10-90}} \sum_{j=1}^{N_{10-90}} |X_{gl,10-90,j} - \bar{X}_{gl,10-90}|$$

$\bar{X}_{gl,10-90}$ denotes the sample mean of $\mathbf{X}_{gl,10-90}$.

2.3.14 Median absolute deviation

Median absolute deviation is similar in concept to $F_{stat.mad}$, but measures dispersion from the median instead of mean. Thus

$$F_{stat.medad} = \frac{1}{N_v} \sum_{j=1}^{N_v} |X_{gl,j} - M|$$

Here, median $M = F_{stat.median}$.

2.3.15 Coefficient of variation

The coefficient of variation measures the dispersion of the \mathbf{X}_{gl} distribution. It is defined as

$$F_{stat.cov} = \frac{\sigma}{\mu}$$

Here $\sigma = F_{stat.var}^{1/2}$ and $\mu = F_{stat.mean}$ are the standard deviation and mean of the grey level distribution, respectively.

2.3.16 Quartile coefficient of dispersion

The quartile coefficient of dispersion is a robust alternative to coefficient of variance. It is defined as

$$F_{stat.qcod} = \frac{P_{75} - P_{25}}{P_{75} + P_{25}}$$

P_{25} and P_{75} are the 25th and 75th percentile of \mathbf{X}_{gl} , respectively.

2.3.17 Energy

The grey level energy of \mathbf{X}_{gl} is defined as:

$$F_{stat.energy} = \sum_{j=1}^{N_v} X_{gl,j}^2$$

2.3.18 Root mean square

The root mean square metric, also called the quadratic mean, of \mathbf{X}_{gl} is defined as:

$$F_{stat.rms} = \sqrt{\frac{\sum_{j=1}^{N_v} X_{gl,j}^2}{N_v}}$$

2.4 Intensity histogram features

An intensity histogram is generated by discretising the original set grey levels \mathbf{X}_{gl} into grey level bins. Approaches to discretisation are described elsewhere in the document. Thus, let $\mathbf{X}_d = \{X_{d,1}, X_{d,2}, \dots, X_{d,N_v}\}$ be the set of discretised grey levels of the N_v voxels in the ROI. Let $\mathbf{H} = \{n_1, n_2, \dots\}$ be the histogram with frequency count n_i of each discretised grey level i in \mathbf{X}_d . The number of grey level bins of the histogram is N_g . The occurrence probability p_i for each grey level bin i is then approximated as $p_i = n_i/N_v$.

Summarising features As with statistical features, assessment of the entire ROI is both the assumed and preferred option. However, in some cases calculation by slice may be required. For example, spatial image filtering may be applied per slice instead of the entire volume. Spatial filtering changes grey level values. After filtering and discretisation consistent meaning of grey values may be lost, if applied by slice. If such a 2 dimensional approach is unavoidable, calculation of features per slice and subsequent averaging is recommended.

2.4.1 Intensity histogram mean

The mean grey level of \mathbf{X}_d is calculated as:

$$F_{ih.mean} = \frac{1}{N_v} \sum_{j=1}^{N_v} X_{d,j}$$

An equivalent formulation is:

$$F_{ih.mean} = \sum_{i=1}^{N_g} i p_i$$

2.4.2 Intensity histogram variance

The variance of \mathbf{X}_d is defined as:

$$F_{ih.var} = \frac{1}{N_v} \sum_{j=1}^{N_v} (X_{d,j} - \mu)^2$$

Here $\mu = F_{ih.mean}$. This formulation is equivalent to:

$$F_{ih.var} = \sum_{i=1}^{N_g} (i - \mu)^2 p_i$$

2.4.3 Intensity histogram skewness

The skewness of \mathbf{X}_d is defined as:

$$F_{ih.skew} = \frac{\frac{1}{N_v} \sum_{j=1}^{N_v} (X_{d,j} - \mu)^3}{\left(\frac{1}{N_v} \sum_{j=1}^{N_v} (X_{d,j} - \mu)^2\right)^{3/2}}$$

Here $\mu = F_{ih.mean}$. This formulation is equivalent to:

$$F_{ih.skew} = \frac{\sum_{i=1}^{N_g} (i - \mu)^3 p_i}{\left(\sum_{i=1}^{N_g} (i - \mu)^2 p_i\right)^{3/2}}$$

If the discretised grey level variance $F_{ih.var} = 0$, $F_{ih.skew} = 0$.

2.4.4 Intensity histogram kurtosis

Kurtosis, or technically excess kurtosis, is calculated as measure of peakedness of the distribution \mathbf{X}_d :

$$F_{ih.kurt} = \frac{\frac{1}{N_v} \sum_{j=1}^{N_v} (X_{d,j} - \mu)^4}{\left(\frac{1}{N_v} \sum_{j=1}^{N_v} (X_{d,j} - \mu)^2\right)^2} - 3$$

Here $\mu = F_{ih.mean}$. The alternative, but equivalent, formulation is:

$$F_{ih.kurt} = \frac{\sum_{i=1}^{N_g} (i - \mu)^4 p_i}{\left(\sum_{i=1}^{N_g} (i - \mu)^2 p_i\right)^2} - 3$$

Note that kurtosis is corrected by a Fisher correction of -3 to center kurtosis on 0 for normal distributions. If the discretised grey level $F_{ih.var} = 0$, $F_{ih.kurt} = 0$.

2.4.5 Intensity histogram median

The median value $F_{ih.median}$ is the sample median of \mathbf{X}_d .

2.4.6 Intensity histogram minimum grey level

The minimum grey level bin is equal to the lowest discretised grey level present in \mathbf{X}_d .

2.4.7 Intensity histogram 10th percentile

P_{10} is the 10th percentile of \mathbf{X}_d .

2.4.8 Intensity histogram 90th percentile

P_{90} is the 90th percentile of \mathbf{X}_d .

2.4.9 Intensity histogram maximum grey level

The maximum grey level is equal to the highest discretised grey level present in \mathbf{X}_d .

2.4.10 Intensity histogram mode

The mode of \mathbf{X}_d is the most common discretised grey level present, i.e. i for which count n_i is maximal. The mode may not be uniquely defined. When multiple bins contain the highest grey level count, the bin closest to the histogram mean is chosen as $F_{ih.mode}$. In pathological cases with two such bins equidistant to the mean, the bin to the left of the mean is selected.

2.4.11 Intensity histogram interquartile range

The interquartile range (IQR) of \mathbf{X}_d is defined as:

$$F_{ih.iqr} = P_{75} - P_{25}$$

P_{25} and P_{75} are the 25th and 75th percentile of \mathbf{X}_d , respectively. The interquartile range of \mathbf{X}_d is always an integer.

2.4.12 Intensity histogram range

The range of grey levels in the histogram is defined as:

$$F_{ih.range} = \max(\mathbf{X}_d) - \min(\mathbf{X}_d)$$

This equal to the width of the histogram.

2.4.13 Intensity histogram mean absolute deviation

The mean absolute deviation is a measure of dispersion from the mean of \mathbf{X}_d :

$$F_{ih.mad} = \frac{1}{N_v} \sum_{i=1}^{N_v} |X_{d,i} - \mu|$$

Here $\mu = F_{ih.mean}$.

2.4.14 Intensity histogram robust mean absolute deviation

The histogram mean absolute deviation can be influenced by outliers, and mean dispersion from the mean could be affected as a consequence. The set of discretised grey levels under consideration can be restricted to those which are closer to the center of the distribution. Let

$$\mathbf{X}_{10-90} = \{x \in \mathbf{X}_d | P_{10}(\mathbf{X}_d) \leq x \leq P_{90}(\mathbf{X}_d)\}$$

Shortly, \mathbf{X}_{10-90} is the set of $N_{10-90} \leq N$ voxels in \mathbf{X}_d whose discretised grey levels are equal to, or lie between, the values corresponding to the 10th and 90th percentiles of \mathbf{X}_d . The robust mean absolute deviation is then:

$$F_{ih.rmad} = \frac{1}{N_{10-90}} \sum_{j=1}^{N_{10-90}} |X_{d,10-90,j} - \bar{X}_{d,10-90}|$$

$\bar{X}_{d,10-90}$ denotes the sample mean of $\mathbf{X}_{d,10-90}$.

2.4.15 Intensity histogram median absolute deviation

Histogram median absolute deviation is similar in concept to $F_{ih.mad}$, but measures dispersion from the median instead of mean. Thus:

$$F_{ih.medmad} = \frac{1}{N_v} \sum_{j=1}^{N_v} |X_{d,j} - M|$$

Here, median $M = F_{ih.median}$.

2.4.16 Intensity histogram coefficient of variation

The coefficient of variation measures the dispersion of the histogram. It is defined as:

$$F_{ih.cov} = \frac{\sigma}{\mu}$$

Here $\sigma = F_{ih.var}^{1/2}$ and $\mu = F_{ih.mean}$ are the standard deviation and mean of the discretised grey level distribution, respectively.

2.4.17 Intensity histogram quartile coefficient of dispersion

The quartile coefficient of dispersion is a robust alternative to coefficient of variance. It is defined as:

$$F_{ih.qcod} = \frac{P_{75} - P_{25}}{P_{75} + P_{25}}$$

P_{25} and P_{75} are the 25th and 75th percentile of \mathbf{X}_d , respectively.

2.4.18 Intensity histogram entropy

Entropy is a information-theoretic concept that gives a metric for the information contained within \mathbf{X}_d . The particular metric used is Shannon entropy, which is defined as:

$$F_{ih.entropy} = - \sum_{i=1}^{N_g} p_i \log_2 p_i$$

2.4.19 Intensity histogram uniformity

Uniformity of \mathbf{X}_d is defined as:

$$F_{ih.uniformity} = \sum_{i=1}^{N_g} p_i^2$$

Note that this feature is also referred to as energy.

2.4.20 Maximum histogram gradient

The histogram gradient can be calculated as:

$$\mathbf{H}' = \left\{ H(2) - H(1), \dots, \frac{H(i+1) - H(i-1)}{2}, \dots, H(N_g) - H(N_g - 1) \right\}$$

Note that this requires a non-sparse representation, i.e. empty bins should be presented. The histogram gradient can ostensibly be calculated in different ways. The suggested method has the advantage of being simple to implement and producing a gradient with same number of elements as the original histogram. The latter helps avoid ambiguity concerning which discretised grey level corresponds to which bin that would occur in simple bin difference gradients. This feature was then defined by van Dijk et al. (2016) as:

$$F_{ih.\max.grad} = \max(\mathbf{H}')$$

2.4.21 Maximum histogram gradient grey level

This feature was defined by van Dijk et al. (2016) as the discretised grey level corresponding to the maximum histogram gradient, i.e. i for which \mathbf{H}' was maximal.

2.4.22 Minimum histogram gradient

This feature was defined by van Dijk et al. (2016) as the minimum gradient of the grey level histogram:

$$F_{ih.\min.grad} = \min(\mathbf{H}')$$

2.4.23 Minimum histogram gradient grey level

This feature was defined by van Dijk et al. (2016) as the discretised grey level corresponding to the minimum histogram gradient, i.e. i for which \mathbf{H}' was minimal.

2.5 Intensity-volume histogram features

The (cumulative) intensity-volume histogram (IVH) of the set of grey levels \mathbf{X}_{gl} of ROI voxels describes the relationship between grey level i and the volume fraction ν which contains at least grey level i or a higher (El Naqa et al., 2009).

The calculation of IVH features requires a discrete grey level ROI voxel set \mathbf{X}_d which contains discrete grey levels from set \mathbf{G} . Depending on the imaging modality, calculation of both \mathbf{X}_d and \mathbf{G} is straightforward, or requires prior discretisation.

Images with discretised grey levels Some images by default contain voxels with discrete intensities, e.g. CT with Hounsfield units. In this case, the discretised ROI voxel set $\mathbf{X}_d = \mathbf{X}_{gl}$. The corresponding set of discretised grey levels $\mathbf{G} = \{\min(\mathbf{X}_d), \min(\mathbf{X}_d) + 1, \dots, \max(\mathbf{X}_d)\}$.

Images requiring discretisation Images without discrete intensities require discretisation. Our general recommendation is to use a *fixed bin number* discretisation method with $N_b = 1000$ bins. The bin number for voxel j is then:

$$X_{b,j} = \begin{cases} 1 & X_{gl,j} = X_{gl,min} \\ \lceil N_b \frac{X_{gl,j} - X_{gl,min}}{X_{gl,max} - X_{gl,min}} \rceil & X_{gl,j} > X_{gl,min} \end{cases}$$

Here, $X_{gl,min} = \min(\mathbf{X}_{gl})$ and $X_{gl,max} = \max(\mathbf{X}_{gl})$ are the minimum and maximum grey level in the ROI. The discrete grey level set for IVH is represented by the bin centres, not bin numbers. Therefore, let $w_b = (X_{gl,max} - X_{gl,min}) / N_b$ be the bin width, and:

$$X_{d,j} = X_{gl,min} + (X_{b,j} - 0.5) w_b$$

The corresponding discretised grey levels are $\mathbf{G} = \{\min(\mathbf{X}_d), \min(\mathbf{X}_d) + w_b, \dots, \max(\mathbf{X}_d)\}$.

In some cases, notably SUV PET images, a more meaningful grey level range can be defined. In SUV PET images the minimum SUV is defined at 0.0, and intensity is related to underlying physiological processes. In such cases, a *fixed bin size* discretisation method may be more appropriate. The bin number of voxel j is then:

$$X_{b,j} = \begin{cases} 1 & X_{gl,j} = X_{gl,min} \\ \lceil \frac{X_{gl,j} - X_{gl,min}}{w_b} \rceil & X_{gl,j} > X_{gl,min} \end{cases}$$

Here w_b and $X_{gl,min}$ are the bin width and minimum grey level parameters respectively. For SUV PET, one may use $w_b = 0.10$ and $X_{gl,min} = 0.00$. As above, the discrete grey level of voxel j is represented by the bin centres:

$$X_{d,j} = X_{gl,min} + (X_{b,j} - 0.5) w_b$$

The corresponding discretised grey levels are $\mathbf{G} = \{\min(\mathbf{X}_d), \min(\mathbf{X}_d) + w_b, \dots, \max(\mathbf{X}_d)\}$.

Calculating the IV histogram From \mathbf{X}_d and \mathbf{G} we calculate fractional volumes and fractional grey levels. As voxels for the same image stack usually all have the same dimensions, we may define fractional volume ν for discrete grey level i in \mathbf{G} as:

$$\nu_i = 1 - \frac{1}{N_v} \sum_{j=1}^{N_v} \delta(X_{d,j} < i)$$

Here δ is the Kronecker delta. In essence, we count the voxels containing a discretised grey level smaller than i , divide by the total number of voxels, and then subtract this volume fraction.

The grey level fraction γ for discrete grey level i in \mathbf{G} is calculated as:

$$\gamma_i = \frac{i - \min(\mathbf{X}_d)}{\max(\mathbf{X}_d) - \min(\mathbf{X}_d)}$$

An example IVH for the digital phantom is shown in Table 2.1.

2.5.1 Volume at intensity fraction

The *volume at intensity fraction* V_x is the largest volume fraction (ν) that has an intensity fraction γ of least $x\%$. This differs from conceptually similar dose-volume histograms used in radiotherapy planning, where V_{10} would indicate the volume fraction receiving at least 10 Gy planned dose. El Naqa et al. (2009) defined both V_{10} and V_{90} as features.

i	γ	ν
1	0.0	1.000
2	0.2	0.324
3	0.4	0.324
4	0.6	0.311
5	0.8	0.095
6	1.0	0.095

Table 2.1: Example intensity-volume histogram evaluated at discrete grey levels i of the digital phantom. γ is the fractional grey level starting at $i = 1$, and with maximum $i = 6$. ν is the corresponding partial volume fraction.

2.5.2 Intensity at volume fraction

The *intensity at volume fraction* I_x is the minimum grey level i present in at most $x\%$ of the volume. El Naqa et al. (2009) defined both I_{10} and I_{90} as features.

2.5.3 Volume at intensity fraction difference

This feature is the difference between the volume fractions at two different intensity fractions, e.g. $V_{10} - V_{90}$ (El Naqa et al., 2009).

2.5.4 Intensity at volume fraction difference

This feature is the difference between grey levels at two different fractional volumes, e.g. $I_{10} - I_{90}$ (El Naqa et al., 2009).

2.5.5 Area under IVH curve

The area under the IVH curve was defined by van Velden et al. (2011). The area under the IVH curve can be approximated by calculating the Riemann sum using the trapezoidal rule. Note that if there is only one grey level in the ROI, $F_{ivh.auc} = 0$.

2.6 Textural features - Grey level co-occurrence based features

In image analysis, texture is one of the defining sets of features. Texture features were originally designed to assess surface texture in 2D images. Texture is not restricted to 2D slices, but may be extended to 3D objects. Image grey levels are generally discretised before calculation of textural features. Approaches to discretisation are described elsewhere in the document.

The grey level co-occurrence matrix (GLCM) is a matrix that expresses how combinations of discretised grey levels of neighbouring pixels, or voxels in a 3D volume, are distributed along one of the image directions. In a 3 dimensional approach to texture analysis, the direct neighbourhood of a voxel consists of the 26 directly neighbouring voxels. Thus, there are 13 unique direction vectors within a neighbourhood volume for distance 1, i.e. $(0, 0, 1)$, $(0, 1, 0)$, $(1, 0, 0)$, $(0, 1, 1)$, $(0, 1, -1)$, $(1, 0, 1)$, $(1, 0, -1)$, $(1, 1, 0)$, $(1, -1, 0)$, $(1, 1, 1)$, $(1, 1, -1)$, $(1, -1, 1)$ and $(1, -1, -1)$.

An alternative approach is to determine the GLCM on image slices, and ignore connections between slices. In this 2 dimensional approach there are only 8 direct neighbours. The corresponding direction vectors at distance 1 are $(1, 0, 0)$, $(1, 1, 0)$, $(0, 1, 0)$ and $(-1, 1, 0)$. A drawback of the 2 dimensional approach is that the resulting features are not geometrically invariant. However, it should also be considered that for many imaging modalities voxel sizes are not isotropic. The in-plane voxel dimensions are usually smaller than the slice thickness. This difference necessitates interpolation between slices to maintain isotropic voxels. At this point in time it is not clear which of the two approaches produces the most robust and effective imaging biomarkers.

A GLCM is calculated for each direction vector, as follows. Let \mathbf{M}_Δ be the $N_g \times N_g$ grey level co-occurrence matrix, where N_g is the number of discretised grey levels present in the volume, and Δ the particular direction. Element (i, j) is the frequency at which combinations of discretised grey levels i and j occur in neighbouring voxels along direction δ and along direction $-\delta$. Then, $\mathbf{M}_\Delta = \mathbf{M}_\delta + \mathbf{M}_{-\delta} = \mathbf{M}_\delta + \mathbf{M}_\delta^T$ (Haralick et al., 1973).

An example for GLCM calculation is shown in Table 2.2. Corresponding grey level co-occurrence matrices for each direction are shown in Table 2.3.

				j				j			
1	2	2	3	0	3	0	0	0	0	0	2
1	2	3	3	i	0	1	3	1	3	1	0
4	2	4	1		0	0	1	0	0	3	1
4	1	2	3		2	1	0	0	0	1	0

Table 2.2: Grey levels (a) and corresponding grey level co-occurrence matrices for the 0° (b) and 180° directions (c). In vector notation these directions are $\delta = (1, 0)$ and $\delta = (-1, 0)$

Grey level co-occurrence matrix features rely on the probability distribution for the elements of the GLCM. Let us consider $\mathbf{M}_{\Delta=(1,0)}$ from the example, as in Table 2.4. We get a probability distribution for grey level co-occurrences, \mathbf{P}_{Δ} , by normalising \mathbf{M}_{Δ} by the sum of its elements. Each element p_{ij} of \mathbf{P}_{Δ} is then the joint probability of grey levels i and j occurring in neighbouring voxels along direction Δ . Then $p_{i\cdot} = \sum_{j=1}^{N_g} p_{ij}$ is the row marginal probability, and $p_{\cdot j} = \sum_{i=1}^{N_g} p_{ij}$ is the column marginal probability. As \mathbf{P}_{Δ} is by definition symmetric, $p_{i\cdot} = p_{\cdot j}$. Furthermore, let us consider diagonal and cross-diagonal probabilities p_{i-j} and p_{i+j} .

$$p_{i-j}(k) = \sum_{i=1}^{N_g} \sum_{j=1}^{N_g} p_{ij} \delta(k - |i - j|) \quad k = 0, \dots, N_g - 1$$

$$p_{i+j}(k) = \sum_{i=1}^{N_g} \sum_{j=1}^{N_g} p_{ij} \delta(k - (i + j)) \quad k = 2, \dots, 2N_g$$

Here, $\delta(x)$ is the Kronecker delta, which equals 1 when $x = 0$ and 0 elsewhere. In calculating diagonal and cross-diagonal probabilities it is used as a filter to select only certain combinations of elements (i, j) .

It should be noted that while a distance d of 1 is commonly used for the GLCM, different distances are possible. For example, for $d = 3$ the voxels at $(0, 0, 3)$, $(0, 3, 0)$, $(3, 0, 0)$, $(0, 3, 3)$, $(0, 3, -3)$, $(3, 0, 3)$, $(3, 0, -3)$, $(3, 3, 0)$, $(3, -3, 0)$, $(3, 3, 3)$, $(3, 3, -3)$, $(3, -3, 3)$ and $(3, -3, -3)$ from the centre voxel are considered.

j				j			
i	0	3	0	2	0	2	0
	3	2	3	2	2	2	1
	0	3	2	0	0	1	2
	2	2	0	0	1	2	1
(a) $\mathbf{M}_{\Delta=\rightarrow}$				(b) $\mathbf{M}_{\Delta=\nearrow}$			
j				j			
i	2	1	2	1	0	2	1
	1	4	1	1	2	2	2
	2	1	2	1	1	2	0
	1	1	1	2	1	1	0
(c) $\mathbf{M}_{\Delta=\uparrow}$				(d) $\mathbf{M}_{\Delta=\nwarrow}$			

Table 2.3: Grey level co-occurrence matrices for the 0° (a), 45° (b), 90° (c) and 135° (d) directions. In vector notation these directions are $\Delta = (1, 0)$, $\Delta = (1, 1)$, $\Delta = (0, 1)$ and $\Delta = (-1, 1)$

Summarising features Feature values are calculated after calculating the grey level co-occurrence matrices and related probability distributions. Five methods can be used to arrive at a single feature value for each volume. A schematic example is shown in Figure 2.2. Three methods involve merging of matrices. By merging the occurrence count for each individual combination of elements (i, j) in the GLCMs is summed. Probability distributions are subsequently calculated using the merged matrix, and features calculated.

2.6.1 Joint maximum

The joint maximum is the probability corresponding to the most common grey level co-occurrence in the GLCM.

$$F_{cm.joint.max} = \max(p_{ij})$$

2.6.2 Joint average

The joint average is the grey level weighted sum of joint probabilities.

$$F_{cm.joint.avg} = \sum_{i=1}^{N_g} \sum_{j=1}^{N_g} i p_{ij}$$

2.6.3 Joint variance

The joint variance, which is also called *sum of squares* (Haralick et al., 1973), is defined as:

$$F_{cm.joint.var} = \sum_{i=1}^{N_g} \sum_{j=1}^{N_g} (i - \mu)^2 p_{ij}$$

Here μ is equal to the value of $F_{cm.joint.avg}$, which was defined previously.

					j	\sum_j										
						0.00	0.13	0.00	0.08	0.21						
					i	0.13	0.08	0.13	0.08	0.42						
					0	0.00	0.13	0.08	0.00	0.21						
					2	0.08	0.08	0.00	0.00	0.17						
\sum_i	5	10	5	4	24	$p_{.j}$	0.21	0.42	0.21	0.17	1.00					

(a) $\mathbf{M}_{\Delta=(1,0)}$ with margins

$k = i - j $	0	1	2	3
p_{i-j}	0.17	0.50	0.17	0.17

(b) $\mathbf{P}_{\Delta=(1,0)}$ with margins

(c) Diagonal probability for $\mathbf{P}_{\Delta=(1,0)}$

$k = i + j$	2	3	4	5	6	7	8
p_{i+j}	0.00	0.25	0.08	0.42	0.25	0.00	0.00

(d) Cross-diagonal probability for $\mathbf{P}_{\Delta=(1,0)}$

Table 2.4: Grey level co-occurrence matrix for the 0° direction (a); its corresponding probability matrix $\mathbf{P}_{\Delta=(1,0)}$ with marginal probabilities $p_{.i}$ and $p_{.j}$ (b); the diagonal probabilities p_{i-j} (c); and the cross-diagonal probabilities p_{i+j} (d). Discrepancies in panels b, c, and d are due to rounding errors. Note that due the matrix symmetry marginal probabilities $p_{.i}$ and $p_{.j}$ are the same in both row and column margins.

2.6.4 Joint entropy

Joint entropy (Haralick et al., 1973) is defined as:

$$F_{cm.joint.entr} = - \sum_{i=1}^{N_g} \sum_{j=1}^{N_g} p_{ij} \log_2 p_{ij}$$

2.6.5 Difference average

The average for the diagonal probabilities is defined as:

$$F_{cm.diff.avg} = \sum_{k=0}^{N_g-1} k p_{i-j}(k)$$

Note that k in $p_{i-j}(k)$ is used as an index for p_{i-j} and does not represent a multiplication.

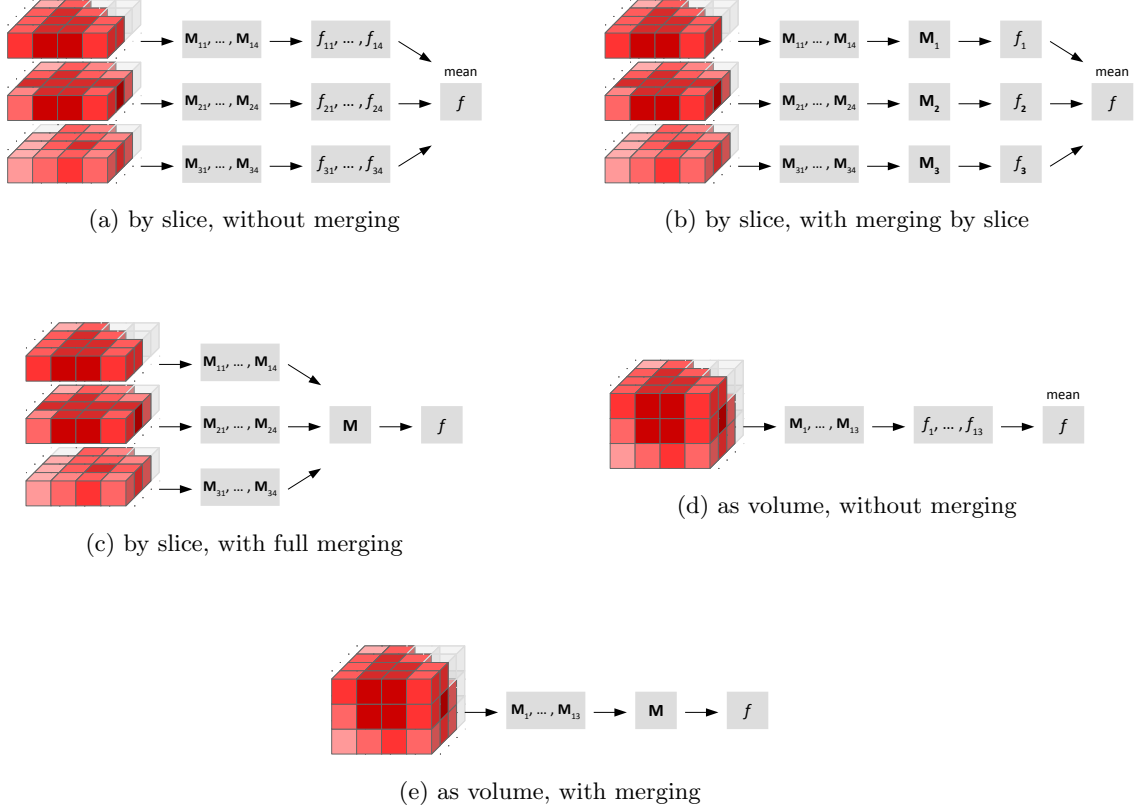


Figure 2.2: Approaches to calculating grey level co-occurrence matrix-based features. $\mathbf{M}_{\Delta k}$ are texture matrices calculated for direction Δ in slice k (if applicable), and $f_{\Delta k}$ is the corresponding feature value. In (b), (c) and (e) the matrices are merged prior to feature calculation.

2.6.6 Difference variance

The variance for the diagonal probabilities (Haralick et al., 1973) is defined as:

$$F_{cm.\text{diff}.var} = \sum_{k=0}^{N_g-1} (k - \mu)^2 p_{i-j}(k)$$

Here μ is equal to the value of $F_{cm.\text{diff}.avg}$.

2.6.7 Difference entropy

The entropy for the diagonal probabilities (Haralick et al., 1973) is defined as:

$$F_{cm.\text{diff}.entr} = - \sum_{k=0}^{N_g-1} p_{i-j}(k) \log_2 p_{i-j}(k)$$

2.6.8 Sum average

The average for the cross-diagonal probabilities (Haralick et al., 1973) is defined as:

$$F_{cm.sum.avg} = \sum_{k=2}^{2N_g} k p_{i+j}(k)$$

2.6.9 Sum variance

The variance for the cross-diagonal probabilities (Haralick et al., 1973) is defined as:

$$F_{cm.sum.var} = \sum_{k=2}^{2N_g} (k - \mu)^2 p_{i+j}(k)$$

Here μ is equal to the value of $F_{cm.sum.avg}$.

2.6.10 Sum entropy

The entropy for the cross-diagonal probabilities (Haralick et al., 1973) is defined as:

$$F_{cm.sum.entr} = - \sum_{k=2}^{2N_g} p_{i+j}(k) \log_2 p_{i+j}(k)$$

2.6.11 Angular second moment

The angular second moment (Haralick et al., 1973), which represent the energy of \mathbf{P}_Δ , is defined as:

$$F_{cm.energy} = \sum_{i=1}^{N_g} \sum_{j=1}^{N_g} p_{ij}^2$$

2.6.12 Contrast

Contrast assesses grey level variations (Haralick et al., 1973). Hence elements of \mathbf{M}_Δ that represent large grey level differences receive greater weight. Contrast is defined as (Clausi, 2002):

$$F_{cm.contrast} = \sum_{i=1}^{N_g} \sum_{j=1}^{N_g} (i - j)^2 p_{ij}$$

Note that the original definition is seemingly more complex, but simplifying terms leads to the above formulation of contrast.

2.6.13 Dissimilarity

Dissimilarity is conceptually similar to the *Contrast* feature, and is defined as:

$$F_{cm.dissimilarity} = \sum_{i=1}^{N_g} \sum_{j=1}^{N_g} |i - j| p_{ij}$$

2.6.14 Inverse difference

Inverse difference is a measure of homogeneity. Grey level co-occurrences with a large difference in levels are weighed less, thus lowering the total feature score. The feature score is maximal if all grey levels are the same. Inverse difference is defined as:

$$F_{cm.\text{inv.}diff} = \sum_{i=1}^{N_g} \sum_{j=1}^{N_g} \frac{p_{ij}}{1 + |i - j|}$$

2.6.15 Inverse difference normalised

Clausi (Clausi, 2002) suggests normalising *inverse difference* to improve classification ability of this feature. This feature is then defined as:

$$F_{cm.\text{inv.}diff.\text{norm}} = \sum_{i=1}^{N_g} \sum_{j=1}^{N_g} \frac{p_{ij}}{1 + |i - j|/N_g}$$

Note that in Clausi's definition, $|i - j|^2/N_g^2$ is used instead of $|i - j|/N_g$, which is likely an oversight, as this exactly the same definition as the *inverse difference moment normalised* function.

2.6.16 Inverse difference moment

Inverse difference moment (Haralick et al., 1973) is similar in concept to the *inverse difference* feature, but with lower weights for elements that are further from the diagonal.

$$F_{cm.\text{inv.}diff.\text{mom}} = \sum_{i=1}^{N_g} \sum_{j=1}^{N_g} \frac{p_{ij}}{1 + (i - j)^2}$$

2.6.17 Inverse difference moment normalised

Clausi (Clausi, 2002) suggests normalising *inverse difference moment* to improve classification performance of this feature. This leads to the following definition:

$$F_{cm.\text{inv.}diff.\text{mom.norm}} = \sum_{i=1}^{N_g} \sum_{j=1}^{N_g} \frac{p_{ij}}{1 + (i - j)^2 / N_g^2}$$

2.6.18 Inverse variance

The inverse variance feature is defined as:

$$F_{cm.\text{inv.}var} = 2 \sum_{i=1}^{N_g} \sum_{j>i}^{N_g} \frac{p_{ij}}{(i - j)^2}$$

2.6.19 Correlation

Correlation (Haralick et al., 1973) is defined as:

$$F_{cm.\text{corr}} = \frac{1}{\sigma_i \cdot \sigma_j} \left(-\mu_i \cdot \mu_j + \sum_{i=1}^{N_g} \sum_{j=1}^{N_g} i j p_{ij} \right)$$

$\mu_{i\cdot} = \sum_{i=1}^{N_g} i p_{i\cdot}$ and $\sigma_{i\cdot} = \left(\sum_{i=1}^{N_g} (i - \mu_{i\cdot})^2 p_{i\cdot} \right)^{1/2}$ are the mean and standard deviation of row marginal probability $p_{i\cdot}$, respectively. Likewise, $\mu_{\cdot j}$ and $\sigma_{\cdot j}$ are the mean and standard deviation column marginal probability $p_{\cdot j}$, respectively. The equation for correlation can be simplified since \mathbf{P}_Δ is symmetrical:

$$F_{cm.corr} = \frac{1}{\sigma_{i\cdot}^2} \left(-\mu_{i\cdot}^2 + \sum_{i=1}^{N_g} \sum_{j=1}^{N_g} i j p_{ij} \right)$$

An equivalent formulation of *correlation* is:

$$F_{cm.corr} = \frac{1}{\sigma_{i\cdot} \sigma_{\cdot j}} \sum_{i=1}^{N_g} \sum_{j=1}^{N_g} (i - \mu_{i\cdot})(j - \mu_{\cdot j}) p_{ij}$$

Again, simplifying due to matrix symmetry yields:

$$F_{cm.corr} = \frac{1}{\sigma_{i\cdot}^2} \sum_{i=1}^{N_g} \sum_{j=1}^{N_g} (i - \mu_{i\cdot})(j - \mu_{i\cdot}) p_{ij}$$

2.6.20 Autocorrelation

Aerts et al. (2014) defined autocorrelation as:

$$F_{cm.auto.corr} = \sum_{i=1}^{N_g} \sum_{j=1}^{N_g} i j p_{ij}$$

2.6.21 Cluster tendency

Cluster tendency is defined as:

$$F_{cm.clust.tend} = \sum_{i=1}^{N_g} \sum_{j=1}^{N_g} (i + j - \mu_{i\cdot} - \mu_{\cdot j})^2 p_{ij}$$

Here $\mu_{i\cdot} = \sum_{i=1}^{N_g} i p_{i\cdot}$ and $\mu_{\cdot j} = \sum_{j=1}^{N_g} j p_{\cdot j}$. Because of the symmetric nature of \mathbf{P}_Δ , the feature can also be formulated as:

$$F_{cm.clust.tend} = \sum_{i=1}^{N_g} \sum_{j=1}^{N_g} (i + j - 2\mu_{i\cdot})^2 p_{ij}$$

2.6.22 Cluster shade

Cluster shade is defined as (Unser, 1986):

$$F_{cm.clust.shade} = \sum_{i=1}^{N_g} \sum_{j=1}^{N_g} (i + j - \mu_{i\cdot} - \mu_{\cdot j})^3 p_{ij}$$

As with *cluster tendency*, $\mu_{i\cdot} = \sum_{i=1}^{N_g} i p_{i\cdot}$ and $\mu_{\cdot j} = \sum_{j=1}^{N_g} j p_{\cdot j}$. Because of the symmetric nature of \mathbf{P}_Δ , the feature can also be formulated as:

$$F_{cm.clust.shade} = \sum_{i=1}^{N_g} \sum_{j=1}^{N_g} (i + j - 2\mu_{i\cdot})^3 p_{ij}$$

2.6.23 Cluster prominence

Cluster prominence is defined as (Unser, 1986):

$$F_{cm.\text{clust.prom}} = \sum_{i=1}^{N_g} \sum_{j=1}^{N_g} (i + j - \mu_{i\cdot} - \mu_{\cdot j})^4 p_{ij}$$

As before, $\mu_{i\cdot} = \sum_{i=1}^{N_g} i p_{i\cdot}$ and $\mu_{\cdot j} = \sum_{j=1}^{N_g} j p_{\cdot j}$. Because of the symmetric nature of \mathbf{P}_Δ , the feature can also be formulated as:

$$F_{cm.\text{clust.prom}} = \sum_{i=1}^{N_g} \sum_{j=1}^{N_g} (i + j - 2\mu_{i\cdot})^4 p_{ij}$$

2.6.24 First measure of information correlation

Information theoretic correlation is estimated using two different measures (Haralick et al., 1973). For symmetric \mathbf{P}_Δ the first measure is defined as:

$$F_{cm.\text{info.corr.1}} = \frac{HXY - HXY_1}{HX}$$

$HXY = - \sum_{i=1}^{N_g} \sum_{j=1}^{N_g} p_{ij} \log_2 p_{ij}$ is the entropy for the joint probability. $HX = - \sum_{i=1}^{N_g} p_{i\cdot} \log_2 p_{i\cdot}$ is the entropy for the row marginal probability, which due to symmetry is equal to the entropy of the column marginal probability. HXY_1 is a type of entropy that is defined as:

$$HXY_1 = - \sum_{i=1}^{N_g} \sum_{j=1}^{N_g} p_{ij} \log_2 (p_{i\cdot} p_{\cdot j})$$

2.6.25 Second measure of information correlation

The second measure of information theoretic correlation is estimated as follows for symmetric \mathbf{P}_Δ :

$$F_{cm.\text{info.corr.2}} = \sqrt{1 - \exp(-2(HXY_2 - HXY))}$$

As earlier, $HXY = - \sum_{i=1}^{N_g} \sum_{j=1}^{N_g} p_{ij} \log_2 p_{ij}$. HXY_2 is a type of entropy defined as:

$$HXY_2 = - \sum_{i=1}^{N_g} \sum_{j=1}^{N_g} p_{i\cdot} p_{\cdot j} \log_2 (p_{i\cdot} p_{\cdot j})$$

If $HXY > HXY_2$, $F_{cm.\text{info.corr.2}} = 0$, as this would otherwise lead to complex numbers.

2.7 Textural features - Grey level run length based features

The grey level run length matrix (GLRLM) was introduced by Galloway (1975) to define various textural features. Like the grey level co-occurrence matrix, GLRLM also assesses the distribution of discretised grey levels in an image or in a stack of images. However, instead of assessing the

combination of levels between neighbouring pixels or voxels, GLRLM assesses grey level run lengths. Run length counts the frequency of consecutive voxels with discretised grey level i along direction Δ .

A complete example for GLRLM construction from a 2D image is shown in Table 2.5. Let \mathbf{M}_Δ be the $N_g \times N_r$ grey level run length matrix, where N_g is the number of discretised grey levels present in the volume and N_r the maximal possible run length along direction Δ . The directions considered are the same as for GLCM. Matrix element $r_{ij} = r(i, j)$ is the number of occurrences where discretised grey level i appears in j consecutive neighbouring voxels or pixels. Then, let N_v be the total number of voxels in the ROI, and $N_s = \sum_{i=1}^{N_g} \sum_{j=1}^{N_r} r_{ij}$ the sum over all elements in \mathbf{M}_Δ . Marginal sums can also be defined. Let $r_{i\cdot}$ be the marginal sum of the runs over run lengths j for grey value i , that is $r_{i\cdot} = \sum_{j=1}^{N_r} r_{ij}$. The marginal sum of the runs over the grey values i for run length j is then $r_{\cdot j} = \sum_{i=1}^{N_g} r_{ij}$.

Summarising features Feature values are calculated after calculating the grey level run length matrices. Five methods can be used to arrive at a single feature value for each volume. A schematic example was shown in Figure 2.2, and applies here as well. Three methods involve merging of matrices. By merging the number of runs for each individual combination of elements (i, j) in the GLRLMs is summed. Features are subsequently calculated from the merged matrix. Note that when matrices are combined, N_v should likewise be summed to retain consistency.

2.7.1 Short runs emphasis

This feature emphasises short run lengths (Galloway, 1975). It is defined as:

$$F_{rlm.sre} = \frac{1}{N_s} \sum_{j=1}^{N_r} \frac{r_{\cdot j}}{j^2}$$

2.7.2 Long runs emphasis

This feature emphasises long run lengths (Galloway, 1975). It is defined as:

$$F_{rlm.lre} = \frac{1}{N_s} \sum_{j=1}^{N_r} j^2 r_{\cdot j}$$

2.7.3 Low grey level run emphasis

This feature is a grey level analogue to $F_{rlm.sre}$ (Chu et al., 1990). Instead of low run lengths, low grey levels are emphasised. The feature is defined as:

$$F_{rlm.lgre} = \frac{1}{N_s} \sum_{i=1}^{N_g} \frac{r_{i\cdot}}{i^2}$$

2.7.4 High grey level run emphasis

The high grey level run emphasis feature is a grey level analogue to $F_{rlm.lre}$ (Chu et al., 1990). The feature emphasises high grey levels, and is defined as:

$$F_{rlm.hgre} = \frac{1}{N_s} \sum_{i=1}^{N_g} i^2 r_{i\cdot}$$

					Run length j										
					1	2	3	4							
					1	4	0	0	0						
i	1	2	3	1	0	0				1	4	0	0	0	
	2	3	2	1	0	0				2	3	1	0	0	
	3	2	1	0	0					3	2	1	0	0	
	4	3	0	0	0					4	3	0	0	0	
					Run length j										
					1	2	3	4							
					1	4	0	0	0						
i	1	2	1	0	0					1	4	0	0	0	
	2	2	0	1	0					2	3	1	0	0	
	3	2	1	0	0					3	4	0	0	0	
	4	1	1	0	0					4	3	0	0	0	
					Run length j										
					1	2	3	4							
					1	4	0	0	0						
i	1	2	1	0	0					1	4	0	0	0	
	2	2	0	1	0					2	3	1	0	0	
	3	2	1	0	0					3	4	0	0	0	
	4	1	1	0	0					4	3	0	0	0	

Table 2.5: Grey level run length matrices for the 0° (a), 45° (b), 90° (c) and 135° (d) directions. In vector notation these directions are $\Delta = (1, 0)$, $\Delta = (1, 1)$, $\Delta = (0, 1)$ and $\Delta = (-1, 1)$

2.7.5 Short run low grey level emphasis

This feature emphasises runs in the upper left quadrant of the GLRLM, where short run lengths and low grey levels are located (Dasarathy and Holder, 1991). It is defined as:

$$F_{rlm.srlge} = \frac{1}{N_s} \sum_{i=1}^{N_g} \sum_{j=1}^{N_r} \frac{r_{ij}}{i^2 j^2}$$

2.7.6 Short run high grey level emphasis

This feature emphasises runs in the lower left quadrant of the GLRLM, where short run lengths and high grey levels are located (Dasarathy and Holder, 1991). The feature is defined as:

$$F_{rlm.srhge} = \frac{1}{N_s} \sum_{i=1}^{N_g} \sum_{j=1}^{N_r} \frac{i^2 r_{ij}}{j^2}$$

2.7.7 Long run low grey level emphasis

This feature emphasises runs in the upper right quadrant of the GLRLM, where long run lengths and low grey levels are located (Dasarathy and Holder, 1991). The feature is defined as:

$$F_{rlm.lrlge} = \frac{1}{N_s} \sum_{i=1}^{N_g} \sum_{j=1}^{N_r} \frac{j^2 r_{ij}}{i^2}$$

2.7.8 Long run high grey level emphasis

This feature emphasises runs in the lower right quadrant of the GLRLM, where long run lengths and high grey levels are located (Dasarathy and Holder, 1991). The feature is defined as:

$$F_{rlm.lrhge} = \frac{1}{N_s} \sum_{i=1}^{N_g} \sum_{j=1}^{N_r} i^2 j^2 r_{ij}$$

2.7.9 Grey level non-uniformity

This feature assesses the distribution of runs over the grey values (Galloway, 1975). The feature value is low when runs are equally distributed along grey levels. The feature is defined as:

$$F_{rlm.glnu} = \frac{1}{N_s} \sum_{i=1}^{N_g} r_i^2$$

2.7.10 Grey level non-uniformity normalised

This is a normalised version of the grey level non-uniformity feature. It is defined as:

$$F_{rlm.glnu.norm} = \frac{1}{N_s^2} \sum_{i=1}^{N_g} r_i^2$$

2.7.11 Run length non-uniformity

This features assesses the distribution of runs over the run lengths (Galloway, 1975). The feature value is low when runs are equally distributed along run lengths. It is defined as:

$$F_{rlm.rlnu} = \frac{1}{N_s} \sum_{j=1}^{N_r} r_{.j}^2$$

2.7.12 Run length non-uniformity normalised

This is normalised version of the run length non-uniformity feature. It is defined as:

$$F_{rlm.rlnu.norm} = \frac{1}{N_s^2} \sum_{j=1}^{N_r} r_{.j}^2$$

2.7.13 Run percentage

This feature assesses the fraction of the number of realised runs and the maximum number of potential runs (Galloway, 1975). Strongly linear or highly uniform ROI volumes produce a low run percentage. It is defined as:

$$F_{rlm.r.perc} = \frac{N_s}{N_v}$$

2.7.14 Grey level variance

This feature estimates the variance in runs for the grey levels. Let $p_{ij} = r_{ij}/N_s$ be the joint probability estimate for finding discretised grey level i with run length j . The feature is then defined as:

$$F_{rlm.gl.var} = \sum_{i=1}^{N_g} \sum_{j=1}^{N_r} (i - \mu)^2 p_{ij}$$

Here, $\mu = \sum_{i=1}^{N_g} \sum_{j=1}^{N_r} i p_{ij}$.

2.7.15 Run length variance

This feature estimates the variance in runs for run lengths. As before let $p_{ij} = r_{ij}/N_s$. The feature is defined as:

$$F_{rlm.rl.var} = \sum_{i=1}^{N_g} \sum_{j=1}^{N_r} (j - \mu)^2 p_{ij}$$

Mean run length is defined as $\mu = \sum_{i=1}^{N_g} \sum_{j=1}^{N_r} j p_{ij}$.

2.7.16 Run entropy

Run entropy was investigated by Albregtsen et al. (2000). Again, let $p_{ij} = r_{ij}/N_s$. The entropy is then defined as:

$$F_{rlm.rl.entr} = - \sum_{i=1}^{N_g} \sum_{j=1}^{N_r} p_{ij} \log_2 p_{ij}$$

2.8 Textural features - Grey level size zone based features

The grey level size zone matrix (GLSZM) counts the number of groups of connected voxels with a specific discretised grey level value and size (Thibault et al., 2014). Voxels are connected if the neighbouring voxel has the same discretised grey level value. Whether a voxel classifies as a neighbour depends on its connectedness. In the 3 dimensional approach to texture analysis we consider 26-connectedness, which indicates that a connection exists if any of the 26 neighbouring voxels shares the grey level of the centre voxel. In the 2 dimensional approach, 8-connectedness is used. An issue with the 2 dimensional approach may be that voxels may be connected across slices, but disconnected within the plane of the slice. Whether this issue negatively affects predictive performance of GLSZM-based features has not been determined.

Let \mathbf{M} be the $N_g \times N_z$ grey level size zone matrix, where N_g is the number of discretised grey levels present in the volume and N_z the maximum zone size of a group, or zone, of connected voxels with the same grey level value. Element $s_{ij} = s(i, j)$ of \mathbf{M} is then number of zones with discretised grey level i and size j . Furthermore, let N_v be the number of voxels and $N_s = \sum_{i=1}^{N_g} \sum_{j=1}^{N_z} s_{ij}$ be the total number of zones. Marginal sums can likewise be defined. Let $s_{i \cdot} = \sum_{j=1}^{N_z} s_{ij}$ be the number of zones with discretised grey level i , regardless of size. Likewise, let $s_{\cdot j} = \sum_{i=1}^{N_g} s_{ij}$ be the number of zones with size j , regardless of grey level. A two dimensional example is shown in Table 2.6.

Summarising features GLSZM feature definitions are based on the definitions of GLRLM features (Thibault et al., 2014). Feature values are calculated after calculating the grey level size zone matrices. Three methods can be used to arrive at a single feature value for each volume. A schematic example is shown in Figure 2.3. One method involves merging of matrices. By merging the number of zones for each individual combination of elements (i, j) in the GLSZMs is summed. Features are subsequently calculated from the merged matrix. Note that when matrices are combined, N_v should likewise be summed to retain consistency.

				Zone size j					
				1	2	3	4	5	
1	2	2	3		1	2	1	0	0
1	2	3	3	i	2	0	0	0	1
4	2	4	1		3	1	0	1	0
4	1	2	3		4	1	1	0	0

(a) Grey levels (b) Grey level size zone matrix

Table 2.6: Original image with grey levels (a); and corresponding grey level distance zone matrix (GLSZM) under 4-connectedness (b). Element $s(i, j)$ of the GLSZM indicates the number of times a zone of j pixels and grey level i occurs within the image.

2.8.1 Small zone emphasis

This feature emphasises small zones. It is defined as:

$$F_{szm.sze} = \frac{1}{N_s} \sum_{j=1}^{N_z} \frac{s_{\cdot j}}{j^2}$$

2.8.2 Large zone emphasis

This feature emphasises large zones. It is defined as:

$$F_{szm.lze} = \frac{1}{N_s} \sum_{j=1}^{N_z} j^2 s_{\cdot j}$$

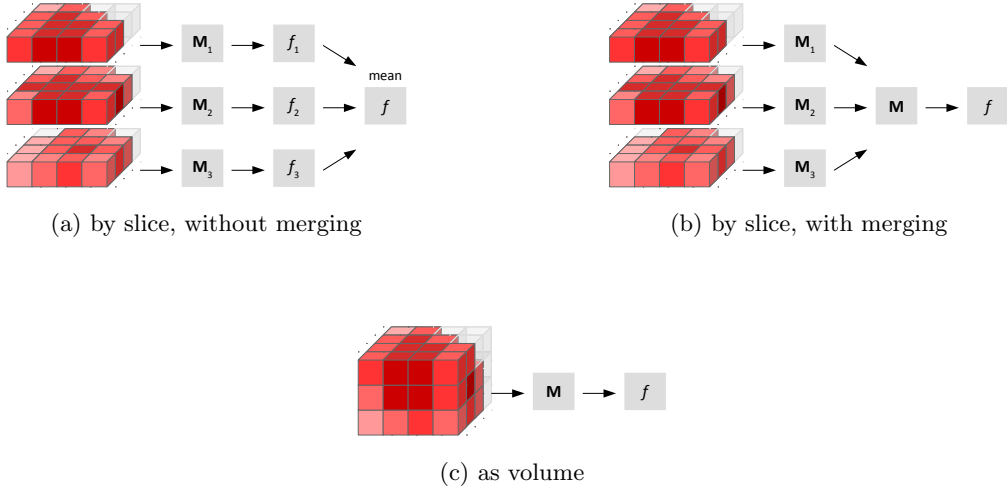


Figure 2.3: Approaches to calculating grey level size zone matrix-based features. \mathbf{M}_k are texture matrices calculated for slice k (if applicable), and f_k is the corresponding feature value. In (b) the matrices from the different slices are merged prior to feature calculation.

2.8.3 Low grey level zone emphasis

This feature is a grey level analogue to $F_{szm.sze}$. Instead of small zone sizes, low grey levels are emphasised. The feature is defined as:

$$F_{szm.lgze} = \frac{1}{N_s} \sum_{i=1}^{N_g} \frac{s_i}{i^2}$$

2.8.4 High grey level zone emphasis

The high grey level zone emphasis feature is a grey level analogue to $F_{szm.lze}$. The feature emphasises high grey levels, and is defined as:

$$F_{szm.hgze} = \frac{1}{N_s} \sum_{i=1}^{N_g} i^2 s_i$$

2.8.5 Small zone low grey level emphasis

This feature emphasises runs in the upper left quadrant of the GLSZM, where small zone sizes and low grey levels are located. It is defined as:

$$F_{szm.szlge} = \frac{1}{N_s} \sum_{i=1}^{N_g} \sum_{j=1}^{N_z} \frac{s_{ij}}{i^2 j^2}$$

2.8.6 Small zone high grey level emphasis

This feature emphasises runs in the lower left quadrant of the GLSZM, where small zone sizes and high grey levels are located. The feature is defined as:

$$F_{szm.szhge} = \frac{1}{N_s} \sum_{i=1}^{N_g} \sum_{j=1}^{N_z} \frac{i^2 s_{ij}}{j^2}$$

2.8.7 Large zone low grey level emphasis

This feature emphasises runs in the upper right quadrant of the GLSZM, where large zone sizes and low grey levels are located. The feature is defined as:

$$F_{szm.lzuge} = \frac{1}{N_s} \sum_{i=1}^{N_g} \sum_{j=1}^{N_z} \frac{j^2 s_{ij}}{i^2}$$

2.8.8 Large zone high grey level emphasis

This feature emphasises runs in the lower right quadrant of the GLSZM, where large zone sizes and high grey levels are located. The feature is defined as:

$$F_{szm.lzhge} = \frac{1}{N_s} \sum_{i=1}^{N_g} \sum_{j=1}^{N_z} i^2 j^2 s_{ij}$$

2.8.9 Grey level non-uniformity

This feature assesses the distribution of zone counts over the grey values. The feature value is low when zone counts are equally distributed along grey levels. The feature is defined as:

$$F_{szm.glnu} = \frac{1}{N_s} \sum_{i=1}^{N_g} s_i^2$$

2.8.10 Grey level non-uniformity normalised

This is a normalised version of the grey level non-uniformity feature. It is defined as:

$$F_{szm.glnu.norm} = \frac{1}{N_s^2} \sum_{i=1}^{N_g} s_i^2$$

2.8.11 Zone size non-uniformity

This feature assesses the distribution of zone counts over the different zone sizes. The feature value is low when zone counts are equally distributed along zone sizes. It is defined as:

$$F_{szm.zsnu} = \frac{1}{N_s} \sum_{j=1}^{N_z} s_j^2$$

2.8.12 Zone size non-uniformity normalised

This is a normalised version of the zone size non-uniformity feature. It is defined as:

$$F_{szm.zsnu.norm} = \frac{1}{N_s^2} \sum_{i=1}^{N_z} s_{.j}^2$$

2.8.13 Zone percentage

This feature assesses the fraction of the number of realised zones and the maximum number of potential zones. Strongly linear or highly uniform ROI volumes produce a low zone percentage. It is defined as:

$$F_{szm.z_perc} = \frac{N_s}{N_v}$$

2.8.14 Grey level variance

This feature estimates the variance in zone counts for the grey levels. Let $p_{ij} = s_{ij}/N_s$ be the joint probability estimate for finding discretised grey level i with zone size j . The feature is then defined as:

$$F_{szm.gl.var} = \sum_{i=1}^{N_g} \sum_{j=1}^{N_z} (i - \mu)^2 p_{ij}$$

Here, $\mu = \sum_{i=1}^{N_g} \sum_{j=1}^{N_z} i p_{ij}$.

2.8.15 Zone size variance

This feature estimates the variance in zone counts for the different zone sizes. As before let $p_{ij} = s_{ij}/N_s$. The feature is defined as:

$$F_{szm.zs.var} = \sum_{i=1}^{N_g} \sum_{j=1}^{N_z} (j - \mu)^2 p_{ij}$$

Mean zone size is defined as $\mu = \sum_{i=1}^{N_g} \sum_{j=1}^{N_z} j p_{ij}$.

2.8.16 Zone size entropy

Let $p_{ij} = s_{ij}/N_s$. Zone size entropy is then defined as:

$$F_{szm.zs.entr} = - \sum_{i=1}^{N_g} \sum_{j=1}^{N_z} p_{ij} \log_2 p_{ij}$$

2.9 Textural features - Neighbourhood grey tone difference based features

Amadasun and King (1989) introduced an alternative grey level matrix. The neighbourhood grey tone difference matrix (NGTDM) contains the sum of grey level differences of pixels/voxels

with discretised grey level i and the average discretised grey level of neighbouring pixels/voxels within a distance d . For 3D volumes, we can extend the original definition by Amadasun and King. Let $X_{dgl}(j_x, j_y, j_z)$ be the discretised grey level of a voxel at position (j_x, j_y, j_z) . Then the average grey level within a neighbourhood centred at (j_x, j_y, j_z) , but excluding (j_x, j_y, j_z) itself is:

$$\begin{aligned}\bar{A}_i &= \bar{A}(j_x, j_y, j_z) \\ &= \frac{1}{W} \sum_{k_z=-d}^d \sum_{k_y=-d}^d \sum_{k_x=-d}^d X_{dgl}(j_x+k_x, j_y+k_y, j_z+k_z) \\ &\quad (k_x, k_y, k_z) \neq (0, 0, 0)\end{aligned}$$

$W = (2d + 1)^3 - 1$ is the size of the neighbourhood. Let n_i be the number of voxels with discretised grey level i that have a complete neighbourhood. Then the entry in the grey tone difference matrix for grey level i is:

$$s_i = \begin{cases} \sum_{i=1}^{n_i} |i - \bar{A}_i| & \text{for } n_i > 0 \\ 0 & \text{for } n_i = 0 \end{cases}$$

A 2D example is shown in Table 2.7. $d = 1$ is used in this example, leading to 8 neighbouring pixels. $s_1 = 0$ because there are no valid pixels with grey level 1. Two pixels have grey level 2. The average value of their neighbours are $19/8$ and $21/8$. Thus $s_2 = |2 - 19/8| + |2 - 21/8| = 1$. Similarly $s_3 = |3 - 19/8| = 0.625$ and $s_4 = |4 - 17/8| = 1.825$.

Note that for practical purposes, we do not require a complete neighbourhood of valid voxels in irregularly shaped volumes. Instead, W is equal to the number of valid voxels in the neighbourhood. Missing voxels receive $X_{dgl} = 0$, and are essentially not counted to determine \bar{A}_i . n_i is then the total number of voxels with grey level i .

Many NGTDM-based features depend on the N_g grey level probabilities $p_i = n_i/N_v$, where N_g is the number of discretised grey levels in the volume and $N_v = \sum n_i$. Furthermore, let $N_{g,p} \leq N_g$ be the number of discretised grey levels with $p_i > 0$. In the above example, $N_g = 4$ and $N_{g,p} = 3$.

Summarising features Feature values are calculated after calculating the neighbourhood grey tone difference matrices. Three methods can be used to arrive at a single feature value for each volume. A schematic example was shown in Figure 2.3, and applies here as well. One method involves merging of matrices. By merging the grey tone difference s_i is summed over the different NGTDMs. Features are subsequently calculated from the merged matrix. Note that when matrices are combined, N_v should likewise be summed to retain consistency.

2.9.1 Coarseness

Grey level differences in coarse textures are generally small due to large-scale patterns. Summing differences gives an indication of the level of the spatial rate of change in intensity (Amadasun and King, 1989). Coarseness is defined as:

$$F_{ngt.coarseness} = \frac{1}{\sum_{i=1}^{N_g} p_i s_i}$$

Because $\sum_{i=1}^{N_g} p_i s_i$ potentially evaluates to 0, the maximum value of $F_{ngt.coarseness}$ is set to an arbitrary number of 10^6 . Amadasun and King originally circumvented this issue by adding a

1	2	2	3
1	2	3	3
4	2	4	1
4	1	2	3

(a) Grey levels

	n_i	p_i	s_i
i	1	0	0.00
	2	2	0.50
	3	1	0.25
	4	1	0.25

(b) Neighbourhood grey tone difference matrix

Table 2.7: Original image with grey levels (a) and corresponding neighbourhood grey tone difference matrix (NGTDM) (b). The N_v pixels with valid neighbours at distance 1 are located within the rectangle in (a). The grey level count n_i , the grey level probability $p_i = n_i/N_v$, and the neighbourhood average grey level s_i for pixels with grey level i . Note that our definition deviates from the original definition of Amadasun and King (1989), which is presented in panels a and b. In our definition fully valid neighbourhood is no longer required. The NGTDM is thus calculated on the entire pixel area, and not solely on those pixels within the rectangle of panel a.

unspecified small number ϵ to the denominator, but an explicit, though arbitrary, maximum value should allow for more consistency.

2.9.2 Contrast

Contrast depends on the dynamic range of the grey levels as well as the spatial frequency of intensity changes (Amadasun and King, 1989). Thus, contrast is defined as:

$$F_{ngt.contrast} = \left(\frac{1}{N_{g,p} (N_{g,p} - 1)} \sum_{i=1}^{N_g} \sum_{j=1}^{N_g} p_i p_j (i - j)^2 \right) \left(\frac{1}{N_v} \sum_{i=1}^{N_g} s_i \right)$$

Grey level probabilities p_i and p_j are copies with different iterators, i.e. $p_i = p_j$ for $i = j$. The first term considers the grey level dynamic range, whereas the second term is a measure for intensity changes within the volume. If $N_{g,p} = 1$, $F_{ngt.contrast} = 0$.

2.9.3 Busyness

Textures with large changes in grey levels between neighbouring voxels are called busy (Amadasun and King, 1989). Busyness was defined as:

$$F_{ngt.busyness} = \frac{\sum_{i=1}^{N_g} p_i s_i}{\sum_{i=1}^{N_g} \sum_{j=1}^{N_g} i p_i - j p_j}, \quad p_i \neq 0 \text{ and } p_j \neq 0$$

As before, $p_i = p_j$ for $i = j$. The original definition was erroneously formulated as the denominator will always evaluate to 0. Therefore we use a slightly different definition:

$$F_{ngt.\text{busyness}} = \frac{\sum_{i=1}^{N_g} p_i s_i}{\sum_{i=1}^{N_g} \sum_{j=1}^{N_g} |ip_i - jp_j|}, \quad p_i \neq 0 \text{ and } p_j \neq 0$$

If $N_{g,p} = 1$, $F_{ngt.\text{busyness}} = 0$.

2.9.4 Complexity

Complex textures are non-uniform and rapid changes in grey levels are common (Amadasun and King, 1989). Texture complexity is defined as:

$$F_{ngt.\text{complexity}} = \frac{1}{N_v} \sum_{i=1}^{N_g} \sum_{j=1}^{N_g} |i - j| \frac{p_i s_i + p_j s_j}{p_i + p_j}, \quad p_i \neq 0 \text{ and } p_j \neq 0$$

As before, $p_i = p_j$ for $i = j$, and likewise $s_i = s_j$ for $i = j$.

2.9.5 Strength

Amadasun and King (1989) defined texture strength as:

$$F_{ngt.\text{strength}} = \frac{\sum_{i=1}^{N_g} \sum_{j=1}^{N_g} (p_i + p_j) (i - j)^2}{\sum_{i=1}^{N_g} s_i}, \quad p_i \neq 0 \text{ and } p_j \neq 0$$

As before, $p_i = p_j$ for $i = j$. If $\sum_{i=1}^{N_g} s_i = 0$, $F_{ngt.\text{strength}} = 0$.

2.10 Textural features - Grey level distance zone based features

The grey level distance zone matrix (GLDZM) counts the number of groups of connected voxels with a specific discretised grey level value and distance to ROI edge (Thibault et al., 2014). The matrix captures the relation between location and grey level. Two maps are required to calculate the GLDZM. The first is a grey level grouping map, identical with the one created for the grey level size zone matrix (GLSZM). The second is a distance map.

Voxels are connected if the neighbouring voxel has the same grey level value. Whether a voxel classifies as a neighbour depends on its connectedness. We consider 26-connectedness for a 3 dimensional approach and 8-connectedness in the 2 dimensional approach for consistency with the GLSZM.

The distance to ROI edge is defined in accordance to 6 or 4-connectedness. Because of the definition of connectedness that is used, the distance of a voxel to the outer border is equal to the minimum number of voxel edges that needs to be crossed along connected voxels to reach the ROI edge. The distance for a connected group of voxels with the same grey value equals the minimum distance in the respective voxels.

Our definition deviates from the original by Thibault et al. (2014). The original was defined in a rectangular 2D image, whereas ROIs are rarely rectangular cuboids. Approximating distance using Chamfer maps is then no longer a fast and easy solution. Determining distance in 6 or 4-connectedness is a relatively efficient solution, as one can step-wise determine distance by starting

at the ROI edge and working inward. A second difference is that the lowest possible distance is 1 instead of 0 for voxels directly on the ROI edge. This prevents division by 0 for some features.

Let \mathbf{D} be the $N_g \times N_d$ grey level size zone matrix, where N_g is the number of discretised grey levels present in the volume and N_d the maximum distance of a group, or zone, of connected voxels with the same discretised grey level value. Element $d_{ij} = d(i, j)$ of \mathbf{D} is then number of zones with discretised grey level i and size j . Furthermore, let N_v be the number of voxels and $N_s = \sum_{i=1}^{N_g} \sum_{j=1}^{N_d} d_{ij}$ be the total number of zones. Marginal sums can likewise be defined. Let $d_{i\cdot} = \sum_{j=1}^{N_d} d_{ij}$ be the number of zones with discretised grey level i , regardless of distance. Likewise, let $d_{\cdot j} = \sum_{i=1}^{N_g} d_{ij}$ be the number of zones with size j , regardless of grey level. A two dimensional example is shown in Table 2.8.

Missing internal voxels The distance map of the GLDZM is affected by the definition of what constitutes the ROI surface. The particular surface used here should match the one used for calculating morphological features. This includes the same treatment of internal missing volumes.

Summarising features Feature values are calculated after calculating the grey level distance zone matrices. Three methods can be used to arrive at a single feature value for each volume. A schematic example was shown in Figure 2.3 and also applies here. One method involve merging of matrices. By merging the number of zones for each individual combination of elements (i, j) in the GLDZMs is summed. Features are subsequently calculated from the merged matrix. Note that when matrices are combined, N_v should likewise be summed to retain consistency.

				d	
				1	2
1	2	2	3	1	1
1	2	3	3	1	2
4	2	4	1	1	2
4	1	2	3	1	1
<hr/>				<hr/>	
(a) Grey levels				(b) Distance map	
<hr/>				<hr/>	
(c) Grey level distance zone matrix				(c) Grey level distance zone matrix	

Table 2.8: Original image with grey levels (a); corresponding distance map for distance to border (b); and corresponding grey level distance zone matrix (GLDZM) under 4-connectedness (b). Element $d(i, j)$ of the GLDZM indicates the number of times a zone with grey level i and a minimum distance to border j occurs within the image.

2.10.1 Small distance emphasis

This feature emphasises small distances. It is defined as:

$$F_{dzm.sde} = \frac{1}{N_s} \sum_{j=1}^{N_d} \frac{d_{\cdot j}}{j^2}$$

2.10.2 Large distance emphasis

This feature emphasises large distances. It is defined as:

$$F_{dzm.lde} = \frac{1}{N_s} \sum_{j=1}^{N_d} j^2 d_{.j}$$

2.10.3 Low grey level zone emphasis

This feature is a grey level analogue to $F_{dzm.sde}$. Instead of small zone distances, low grey levels are emphasised. The feature is defined as:

$$F_{dzm.lgze} = \frac{1}{N_s} \sum_{i=1}^{N_g} \frac{d_i}{i^2}$$

2.10.4 High grey level zone emphasis

The high grey level zone emphasis feature is a grey level analogue to $F_{dzm.lde}$. The feature emphasises high grey levels, and is defined as:

$$F_{dzm.hgze} = \frac{1}{N_s} \sum_{i=1}^{N_g} i^2 d_i$$

2.10.5 Small distance low grey level emphasis

This feature emphasises runs in the upper left quadrant of the GLDZM, where small zone distances and low grey levels are located. It is defined as:

$$F_{dzm.sdlge} = \frac{1}{N_s} \sum_{i=1}^{N_g} \sum_{j=1}^{N_d} \frac{d_{ij}}{i^2 j^2}$$

2.10.6 Small distance high grey level emphasis

This feature emphasises runs in the lower left quadrant of the GLDZM, where small zone distances and high grey levels are located. The feature is defined as:

$$F_{dzm.sdhge} = \frac{1}{N_s} \sum_{i=1}^{N_g} \sum_{j=1}^{N_d} \frac{i^2 d_{ij}}{j^2}$$

2.10.7 Large distance low grey level emphasis

This feature emphasises runs in the upper right quadrant of the GLDZM, where large zone distances and low grey levels are located. The feature is defined as:

$$F_{dzm.ldlge} = \frac{1}{N_s} \sum_{i=1}^{N_g} \sum_{j=1}^{N_d} \frac{j^2 d_{ij}}{i^2}$$

2.10.8 Large distance high grey level emphasis

This feature emphasises runs in the lower right quadrant of the GLDZM, where large zone distances and high grey levels are located. The feature is defined as:

$$F_{dzm.ldhge} = \frac{1}{N_s} \sum_{i=1}^{N_g} \sum_{j=1}^{N_d} i^2 j^2 d_{ij}$$

2.10.9 Grey level non-uniformity

This feature assesses the distribution of zone counts over the grey values. The feature value is low when zone counts are equally distributed along grey levels. The feature is defined as:

$$F_{dzm.glnu} = \frac{1}{N_s} \sum_{i=1}^{N_g} d_i^2$$

2.10.10 Grey level non-uniformity normalised

This is a normalised version of the grey level non-uniformity feature. It is defined as:

$$F_{dzm.glnu.norm} = \frac{1}{N_s^2} \sum_{i=1}^{N_g} d_i^2$$

2.10.11 Zone distance non-uniformity

This features assesses the distribution of zone counts over the different zone distances. The feature value is low when zone counts are equally distributed along zone distances. It is defined as:

$$F_{dzm.zdnu} = \frac{1}{N_s} \sum_{j=1}^{N_d} d_{.j}^2$$

2.10.12 Zone distance non-uniformity normalised

This is a normalised version of the zone distance non-uniformity feature. It is defined as:

$$F_{dzm.zdnu.norm} = \frac{1}{N_s^2} \sum_{i=1}^{N_d} d_{.i}^2$$

2.10.13 Zone percentage

This feature assesses the fraction of the number of realised zones and the maximum number of potential zones. Strongly linear or highly uniform ROI volumes produce a low zone percentage. It is defined as:

$$F_{dzm.z_perc} = \frac{N_s}{N_v}$$

2.10.14 Grey level variance

This feature estimates the variance in zone counts for the grey levels. Let $p_{ij} = d_{ij}/N_s$ be the joint probability estimate for finding zones with discretised grey level i at distance j . The feature is then defined as:

$$F_{dzm.gl.var} = \sum_{i=1}^{N_g} \sum_{j=1}^{N_d} (i - \mu)^2 p_{ij}$$

Here, $\mu = \sum_{i=1}^{N_g} \sum_{j=1}^{N_d} i p_{ij}$.

2.10.15 Zone distance variance

This feature estimates the variance in zone counts for the different zone distances. As before let $p_{ij} = d_{ij}/N_s$. The feature is defined as:

$$F_{dzm.zd.var} = \sum_{i=1}^{N_g} \sum_{j=1}^{N_d} (j - \mu)^2 p_{ij}$$

Mean zone size is defined as $\mu = \sum_{i=1}^{N_g} \sum_{j=1}^{N_d} j p_{ij}$.

2.10.16 Zone distance entropy

Let $p_{ij} = d_{ij}/N_s$. Zone distance entropy is then defined as:

$$F_{dzm.zd.entr} = - \sum_{i=1}^{N_g} \sum_{j=1}^{N_d} p_{ij} \log_2 p_{ij}$$

2.11 Textural features - Neighbouring grey level dependence based features

Sun and Wee (1983) defined the neighbouring grey level dependence matrix (NGLDM) as an alternative to the grey level co-occurrence matrix. The NGLDM captures the coarseness of the overall texture and is rotationally invariant.

To construct the NGLDM a neighbourhood is defined as the voxels located within a distance d around a centre voxel. The discretised grey levels of the centre voxel c and a neighbouring voxel m are said to be dependent if $|X_{gl,c} - X_{gl,m}| \leq a$, with a being a positive integer coarseness parameter. The number of grey level dependent voxels in the neighbourhood are then counted. This is iteratively done for every voxel. \mathbf{M} is then the $N_g \times N_n$ neighbouring grey level dependence matrix, where N_g is the number of discretised grey levels present in the volume and N_n the maximum grey level dependence count present. Element $s_{ij} = s(i, j)$ of \mathbf{M} is then the number of neighbourhoods with centre voxel discretised grey level i and dependence $k = j - 1$. Since a dependence $k = 0$ is possible, iterator j has to be explicitly defined as $j = k + 1$. Furthermore, let N_v be the number of voxels in the volume, and $N_s = \sum_{i=1}^{N_g} \sum_{j=1}^{N_n} s_{ij}$ the number of neighbourhoods. Marginal sums can likewise be defined. Let $s_{i \cdot} = \sum_{j=1}^{N_n} s_{ij}$ be the number of neighbourhoods with discretised grey level i , essentially constituting a grey level histogram of the volume or slice. Let $s_{\cdot j} = \sum_{i=1}^{N_g} s_{ij}$ be the number of neighbourhoods with dependence j , regardless of grey level. A two dimensional example is shown in Table 2.9.

The definition we use deviates from the original by Sun and Wee (1983). Because regions of interest are rarely cuboid, omission of neighbourhoods which contain voxels beyond the ROI edge may lead to inconsistent results, especially for larger d . Hence the neighbourhoods of all voxels in the volume or slice within the ROI are considered, and consequently $N_v = N_s$. Neighbourhood voxels located outside the ROI do not add to dependence j . Thus, small and tortuous ROI will be considered coarser as neighbouring grey level dependence j is low.

Note that while $a = 0$ is a typical choice for the coarseness parameter, different a are possible. For consistency it may be beneficial to keep $a = 0$ and change grey levels through a discretisation procedure. Likewise, a typical choice for neighbourhood radius is $d = 1$, or rather $d = \sqrt{3}$, but larger values may be useful as well.

The NGLDM-based features are analogous to that of the grey level run length matrix, grey level size zone matrix and grey level distance zone matrix, and expand on the set defined by Sun and Wee (1983).

Summarising features Feature values are calculated after calculating the neighbouring grey level dependence matrices. Three methods can be used to arrive at a single feature value for each volume. A schematic example was shown in Figure 2.3, and applies here as well. One method involve merging of matrices. By merging the number of neighbourhoods for each individual combination of elements (i, j) in the NGLDMs is summed. Features are subsequently calculated from the merged matrix. Note that when matrices are combined, N_v should likewise be summed to retain consistency.

				dependence k
				0 1 2 3
1	2	2	3	1 0 0 0 0
1	2	3	3	i 2 0 0 1 1
4	2	4	1	3 0 0 1 0
4	1	2	3	4 1 0 0 0

(a) Grey levels (b) Neighbouring grey level dependence matrix

Table 2.9: Original image with grey levels and pixels with a complete neighbourhood within the square (a); corresponding neighbouring grey level dependence matrix for distance $d = \sqrt{2}$ and coarseness parameter $a = 0$ (b). Element $s(i, j)$ of the NGLDM indicates the number of neighbourhoods with a centre pixel with grey level i and neighbouring grey level dependence k within the image. Note that in practice we no longer require a complete neighbourhood. Thus every voxel is considered as a centre voxel with a neighbourhood, instead of being constrained to the voxels within the square in panel (a).

2.11.1 Low dependence emphasis

This feature emphasises low neighbouring grey level dependence counts. Sun and Wee (1983) refer to this feature as *Small number emphasis*. It is defined as:

$$F_{ngl.lde} = \frac{1}{N_s} \sum_{j=1}^{N_n} \frac{s_{,j}}{j^2}$$

2.11.2 High dependence emphasis

This feature emphasises high neighbouring grey level dependence counts. Sun and Wee (1983) refer to this feature as *Large number emphasis*. It is defined as:

$$F_{ngl.hde} = \frac{1}{N_s} \sum_{j=1}^{N_n} j^2 s_{.j}$$

2.11.3 Low grey level count emphasis

This feature is a grey level analogue to $F_{ngl.lde}$. Instead of low neighbouring grey level dependence counts, low grey levels are emphasised. The feature is defined as:

$$F_{ngl.lgce} = \frac{1}{N_s} \sum_{i=1}^{N_g} \frac{s_{i.}}{i^2}$$

2.11.4 High grey level count emphasis

The high grey level count emphasis feature is a grey level analogue to $F_{ngl.hde}$. The feature emphasises high grey levels, and is defined as:

$$F_{ngl.hgce} = \frac{1}{N_s} \sum_{i=1}^{N_g} i^2 s_{i.}$$

2.11.5 Low dependence low grey level emphasis

This feature emphasises neighbouring grey level dependence counts in the upper left quadrant of the NGLDM, where low dependence counts and low grey levels are located. It is defined as:

$$F_{ngl.ldlge} = \frac{1}{N_s} \sum_{i=1}^{N_g} \sum_{j=1}^{N_n} \frac{s_{ij}}{i^2 j^2}$$

2.11.6 Low dependence high grey level emphasis

This feature emphasises neighbouring grey level dependence counts in the lower left quadrant of the NGLDM, where low dependence counts and high grey levels are located. The feature is defined as:

$$F_{ngl.ldhge} = \frac{1}{N_s} \sum_{i=1}^{N_g} \sum_{j=1}^{N_n} \frac{i^2 s_{ij}}{j^2}$$

2.11.7 High dependence low grey level emphasis

This feature emphasises neighbouring grey level dependence counts in the upper right quadrant of the NGLDM, where high dependence counts and low grey levels are located. The feature is defined as:

$$F_{ngl.hdlge} = \frac{1}{N_s} \sum_{i=1}^{N_g} \sum_{j=1}^{N_n} \frac{j^2 s_{ij}}{i^2}$$

2.11.8 High dependence high grey level emphasis

This feature emphasises neighbouring grey level dependence counts in the lower right quadrant of the NGLDM, where high dependence counts and high grey levels are located. The feature is defined as:

$$F_{ngl.hdhge} = \frac{1}{N_s} \sum_{i=1}^{N_g} \sum_{j=1}^{N_n} i^2 j^2 s_{ij}$$

2.11.9 Grey level non-uniformity

This feature assesses the distribution of neighbouring grey level dependence counts over the grey values. The feature value is low when dependence counts are equally distributed along grey levels. The feature is defined as:

$$F_{ngl.glnu} = \frac{1}{N_s} \sum_{i=1}^{N_g} s_i^2$$

2.11.10 Grey level non-uniformity normalised

This is a normalised version of the grey level non-uniformity feature. It is defined as:

$$F_{ngl.glnu.norm} = \frac{1}{N_s^2} \sum_{i=1}^{N_g} s_i^2$$

2.11.11 Dependence count non-uniformity

This features assesses the distribution of neighbouring grey level dependence counts over the different dependence counts. The feature value is low when dependence counts are equally distributed. Sun and Wee (1983) refer to this feature as *Number nonuniformity*. It is defined as:

$$F_{ngl.dcnu} = \frac{1}{N_s} \sum_{j=1}^{N_n} s_{.j}^2$$

2.11.12 Dependence count non-uniformity normalised

This is a normalised version of the dependence count non-uniformity feature. It is defined as:

$$F_{ngl.dcnu.norm} = \frac{1}{N_s^2} \sum_{j=1}^{N_n} s_{.j}^2$$

2.11.13 Dependence count percentage

This feature assesses the fraction of the number of realised neighbourhoods and the maximum number of potential neighbourhoods. The feature may be omitted as it evaluates to 1 when complete neighbourhoods are not required, which is the case under our definition. It is defined as:

$$F_{ngl.dc_perc} = \frac{N_s}{N_v}$$

2.11.14 Grey level variance

This feature estimates the variance in dependence counts for the grey levels. Let $p_{ij} = s_{ij}/N_s$ be the joint probability estimate for finding discretised grey level i with dependence j . The feature is then defined as:

$$F_{ngl.gl.var} = \sum_{i=1}^{N_g} \sum_{j=1}^{N_n} (i - \mu)^2 p_{ij}$$

Here, $\mu = \sum_{i=1}^{N_g} \sum_{j=1}^{N_n} i p_{ij}$.

2.11.15 Dependence count variance

This feature estimates the variance in dependence counts for the different dependence counts possible. As before let $p_{ij} = s_{ij}/N_s$. The feature is defined as:

$$F_{ngl.dc.var} = \sum_{i=1}^{N_g} \sum_{j=1}^{N_n} (j - \mu)^2 p_{ij}$$

Mean dependence count is defined as $\mu = \sum_{i=1}^{N_g} \sum_{j=1}^{N_n} j p_{ij}$.

2.11.16 Dependence count entropy

This feature is referred to as *Entropy* by Sun and Wee (1983). Let $p_{ij} = s_{ij}/N_s$. Dependence count entropy is then defined as:

$$F_{ngl.dc.entr} = - \sum_{i=1}^{N_g} \sum_{j=1}^{N_n} p_{ij} \log_2 p_{ij}$$

This definition remedies an error in the original definition, where the term within the logarithm is dependence count s_{ij} instead of count probability p_{ij} .

2.11.17 Dependence count energy

This feature is called *second moment* by Sun and Wee (1983). Let $p_{ij} = s_{ij}/N_s$. Then dependence count energy is defined as:

$$F_{ngl.dc.energy} = \sum_{i=1}^{N_g} \sum_{j=1}^{N_n} p_{ij}^2$$

This definition remedies an error in the original definition. There squared dependence count s_{ij}^2 is normalised only by N_s , thus leaving a major volume dependency. Here we effectively normalise s_{ij}^2 by N_s^2 .

Bibliography

- Aerts, H. J. W. L., Rios-Velazquez, E., Leijenaar, R. T. H., Parmar, C., Grossmann, P., Cavalho, S., Bussink, J., Monshouwer, R., Haibe-Kains, B., Rietveld, D., Hoebers, F. J. P., Rietbergen, M. M., Leemans, C. R., Dekker, A., Quackenbush, J., Gillies, R. J., and Lambin, P. (2014). Decoding tumour phenotype by noninvasive imaging using a quantitative radiomics approach. *Nature communications*, 5:4006.
- Ahipaaolu, S. D. (2015). Fast algorithms for the minimum volume estimator. *Journal of Global Optimization*, 62(2):351–370.
- Albregtsen, F., Nielsen, B., and Danielsen, H. (2000). Adaptive gray level run length features from class distance matrices. In *Proceedings 15th International Conference on Pattern Recognition. ICPR-2000*, volume 3, pages 738–741. IEEE Comput. Soc.
- Amadasun, M. and King, R. (1989). Textural features corresponding to textural properties. *IEEE Transactions on Systems, Man and Cybernetics*, 19(5):1264–1273.
- Barequet, G. and Har-Peled, S. (2001). Efficiently Approximating the Minimum-Volume Bounding Box of a Point Set in Three Dimensions. *Journal of Algorithms*, 38(1):91–109.
- Chan, C. and Tan, S. (2001). Determination of the minimum bounding box of an arbitrary solid: an iterative approach. *Computers and Structures*, 79(15):1433–1449.
- Chu, A., Sehgal, C. M., and Greenleaf, J. F. (1990). Use of gray value distribution of run lengths for texture analysis. *Pattern Recognition Letters*, 11(6):415–419.
- Clausi, D. A. (2002). An analysis of co-occurrence texture statistics as a function of grey level quantization. *Canadian Journal of Remote Sensing*, 28(1):45–62.
- Da Silva, E. C., Silva, A. C., De Paiva, A. C., and Nunes, R. A. (2008). Diagnosis of lung nodule using Moran's index and Geary's coefficient in computerized tomography images. *Pattern Analysis and Applications*, 11(1):89–99.
- Dale, M. R. T., Dixon, P., Fortin, M.-J., Legendre, P., Myers, D. E., and Rosenberg, M. S. (2002). Conceptual and mathematical relationships among methods for spatial analysis. *Ecography*, 25(5):558–577.
- Dasarathy, B. V. and Holder, E. B. (1991). Image characterizations based on joint gray level run length distributions. *Pattern Recognition Letters*, 12(8):497–502.
- El Naqa, I., Grigsby, P. W., Apte, A., Kidd, E., Donnelly, E., Khullar, D., Chaudhari, S., Yang, D., Schmitt, M., Laforest, R., Thorstad, W. L., and Deasy, J. O. (2009). Exploring feature-based approaches in PET images for predicting cancer treatment outcomes. *Pattern recognition*, 42(6):1162–1171.

- Galloway, M. M. (1975). Texture analysis using gray level run lengths. *Computer Graphics and Image Processing*, 4(2):172–179.
- Geary, R. C. (1954). The Contiguity Ratio and Statistical Mapping. *The Incorporated Statistician*, 5(3):115–145.
- Gillies, R. J., Kinahan, P. E., and Hricak, H. (2015). Radiomics: Images Are More than Pictures, They Are Data. *Radiology*, 278(2):151169.
- Haralick, R. M., Shanmugam, K., and Dinstein, I. (1973). Textural Features for Image Classification. *IEEE Transactions on Systems, Man, and Cybernetics*, 3(6):610–621.
- Hatt, M., Majdoub, M., Vallières, M., Tixier, F., Le Rest, C. C., Groheux, D., Hindié, E., Martineau, A., Pradier, O., Hustinx, R., Perdrisot, R., Guillevin, R., El Naqa, I., and Visvikis, D. (2015). 18F-FDG PET uptake characterization through texture analysis: investigating the complementary nature of heterogeneity and functional tumor volume in a multi-cancer site patient cohort. *Journal of nuclear medicine*, 56(1):38–44.
- Hatt, M., Tixier, F., Pierce, L., Kinahan, P. E., Le Rest, C. C., and Visvikis, D. (2016). Characterization of PET/CT images using texture analysis: the past, the present... any future? *European journal of nuclear medicine and molecular imaging*.
- Heiberger, R. M. and Holland, B. (2015). *Statistical Analysis and Data Display*. Springer Texts in Statistics. Springer New York, New York, NY.
- Khachiyan, L. G. (1996). Rounding of Polytopes in the Real Number Model of Computation. *Mathematics of Operations Research*, 21(2):307–320.
- Kumar, V., Gu, Y., Basu, S., Berglund, A. E., Eschrich, S. A., Schabath, M. B., Forster, K., Aerts, H. J. W. L., Dekker, A., Fenstermacher, D., Goldgof, D. B., Hall, L. O., Lambin, P., Balagurunathan, Y., Gatenby, R. A., and Gillies, R. J. (2012). Radiomics: the process and the challenges. *Magnetic Resonance Imaging*, 30(9):1234–1248.
- Lambin, P., Rios-Velazquez, E., Leijenaar, R. T. H., Carvalho, S., van Stiphout, R. G. P. M., Granton, P., Zegers, C. M. L., Gillies, R. J., Boellard, R., Dekker, A., and Aerts, H. J. W. L. (2012). Radiomics: Extracting more information from medical images using advanced feature analysis. *European Journal of Cancer*, 48(4):441–446.
- Lewiner, T., Lopes, H., Vieira, A. W., and Tavares, G. (2003). Efficient Implementation of Marching Cubes' Cases with Topological Guarantees. *Journal of Graphics Tools*, 8(2):1–15.
- Lorensen, W. E. and Cline, H. E. (1987). Marching cubes: A high resolution 3D surface construction algorithm. *ACM SIGGRAPH Computer Graphics*, 21(4):163–169.
- Mazurowski, M. A., Czarnek, N. M., Collins, L. M., Peters, K. B., and Clark, K. (2016). Predicting outcomes in glioblastoma patients using computerized analysis of tumor shape: preliminary data. In Tourassi, G. D. and Armato, S. G., editors, *SPIE Medical Imaging*, volume 9785, page 97852T.
- Moran, P. A. P. (1950). Notes on continuous stochastic phenomena. *Biometrika*, 37:17–23.
- O'Rourke, J. (1985). Finding minimal enclosing boxes. *International Journal of Computer and Information Sciences*, 14(3):183–199.

- Stelldinger, P., Latecki, L. J., and Siqueira, M. (2007). Topological equivalence between a 3D object and the reconstruction of its digital image. *IEEE transactions on pattern analysis and machine intelligence*, 29(1):126–40.
- Sun, C. and Wee, W. G. (1983). Neighboring gray level dependence matrix for texture classification. *Computer Vision, Graphics, and Image Processing*, 23(3):341–352.
- Thibault, G., Angulo, J., and Meyer, F. (2014). Advanced statistical matrices for texture characterization: application to cell classification. *IEEE transactions on bio-medical engineering*, 61(3):630–7.
- Todd, M. J. and Yldrm, E. A. (2007). On Khachiyan’s algorithm for the computation of minimum-volume enclosing ellipsoids. *Discrete Applied Mathematics*, 155(13):1731–1744.
- Unser, M. (1986). Sum and difference histograms for texture classification. *IEEE transactions on pattern analysis and machine intelligence*, 8(1):118–125.
- Vaidya, M., Creach, K. M., Frye, J., Dehdashti, F., Bradley, J. D., and El Naqa, I. (2012). Combined PET/CT image characteristics for radiotherapy tumor response in lung cancer. *Radiotherapy and oncology*, 102(2):239–45.
- van Dijk, L. V., Brouwer, C. L., van der Schaaf, A., Burgerhof, J. G., Beukinga, R. J., Langendijk, J. A., Sijtsema, N. M., and Steenbakkers, R. J. (2016). CT image biomarkers to improve patient-specific prediction of radiation-induced xerostomia and sticky saliva. *Radiotherapy and Oncology*, page submitted.
- van Velden, F. H. P., Cheebsumon, P., Yaqub, M., Smit, E. F., Hoekstra, O. S., Lammertsma, A. A., and Boellaard, R. (2011). Evaluation of a cumulative SUV-volume histogram method for parameterizing heterogeneous intratumoural FDG uptake in non-small cell lung cancer PET studies. *European journal of nuclear medicine and molecular imaging*, 38(9):1636–47.
- Wahl, R. L., Jacene, H., Kasamon, Y., and Lodge, M. A. (2009). From RECIST to PERCIST: Evolving Considerations for PET response criteria in solid tumors. *Journal of nuclear medicine*, 50 Suppl 1(5):122S–50S.
- Weisstein, E. W. (2016). Ellipsoid, <http://mathworld.wolfram.com/Ellipsoid.html>.
- Yip, S. S. F. and Aerts, H. J. W. L. (2016). Applications and limitations of radiomics. *Physics in medicine and biology*, 61(13):R150–66.
- Zhang, C. and Chen, T. (2001). Efficient feature extraction for 2D/3D objects in mesh representation. In *Proceedings 2001 International Conference on Image Processing*, volume 2, pages 935–938. IEEE.